Cell Reports

Article

NCOA4 links iron bioavailability to DNA metabolism

Graphical abstract

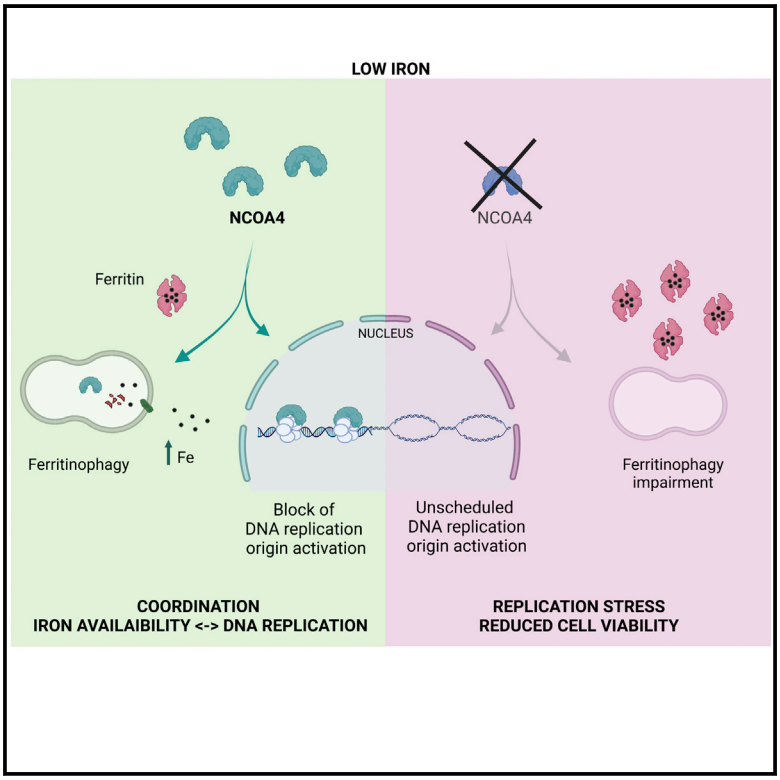

Highlights

- Adequate iron availability is required for proper DNA replication
- Mammalian cells react to low iron by preventing initiation of DNA replication
- Low iron promotes NCOA4 binding to replication origins to prevent their activation
- Lack of NCOA4 causes unscheduled origin activation and replication stress

Authors

Giorgia Federico, Federica Carrillo, Francesca Dapporto, Mario Chiariello, Massimo Santoro, Roberto Bellelli, Francesca Carlomagno

Correspondence

francesca.carlomagno@unina.it

In brief

Federico et al. show that under low-iron conditions, NCOA4 binds to DNA replication origins to block their activation and prevent replication stress. Such a checkpoint preserves cell viability *in vitro* and sustains tissue regeneration in response to dextran sulfate sodium-mediated intestine injury in living animals.

Federico et al., 2022, Cell Reports *40*, 111207
August 16, 2022
https://doi.org/10.1016/j.celrep.2022.111207

CellPress

Cell Reports

CellPress
OPEN ACCESS

Article

NCOA4 links iron bioavailability to DNA metabolism

Giorgia Federico,[1] Federica Carrillo,[1] Francesca Dapporto,[2] Mario Chiariello,[2] Massimo Santoro,[1] Roberto Bellelli,[3] and Francesca Carlomagno[1,4,*]

[1]Department of Molecular Medicine and Medical Biotechnology (DMMBM), University of Naples Federico II, via Sergio Pansini 5, Naples 80131, Italy

[2]Istituto di Fisiologia Clinica (IFC), Consiglio Nazionale delle Ricerche (CNR) and Core Research Laboratory (CRL), Istituto per lo Studio, la Prevenzione e la Rete Oncologica (ISPRO), Siena 53100, Italy

[3]Centre for Cancer Cell and Molecular Biology, Barts Cancer Institute, Charterhouse Square, Barbican, London EC1M 6BE, UK

[4]Lead contact

*Correspondence: francesca.carlomagno@unina.it

https://doi.org/10.1016/j.celrep.2022.111207

SUMMARY

Iron is essential for deoxyribonucleotides production and for enzymes containing an Fe-S cluster involved in DNA replication and repair. How iron bioavailability and DNA metabolism are coordinated remains poorly understood. NCOA4 protein mediates autophagic degradation of ferritin to maintain iron homeostasis and inhibits DNA replication origin activation via hindrance of the MCM2-7 DNA helicase. Here, we show that iron deficiency inhibits DNA replication, parallel to nuclear NCOA4 stabilization. In iron-depleted cells, NCOA4 knockdown leads to unscheduled DNA synthesis, with replication stress, genome instability, and cell death. In mice, NCOA4 genetic inactivation causes defective intestinal regeneration upon dextran sulfate sodium-mediated injury, with DNA damage, defective cell proliferation, and cell death; in intestinal organoids, this is fostered by iron depletion. In summary, we describe a NCOA4-dependent mechanism that coordinates iron bioavailability and DNA replication. This function prevents replication stress, maintains genome integrity, and sustains high rates of cell proliferation during tissue regeneration.

INTRODUCTION

Iron is a trace element required for fundamental metabolic processes in eukaryotes. In addition to its well-established role in oxygen transport and hematopoiesis, iron is crucial for deoxyribonucleotide (dNTPs) synthesis and DNA replication. Thus, the regulatory subunit of the mammalian ribonucleotide reductase (RRM2) forms a diferric-tyrosyl radical cofactor (Fe^{III}_2-Y) necessary for reduction of nucleotides to dNTPs, a limiting step for DNA synthesis and maintenance of genome integrity (Elledge et al., 1992). Moreover, iron participates in a variety of biological processes, such as electron transport, tricarboxylic acid (TCA) cycle, amino acid biosynthesis, tRNA modification in the cytosol, and DNA metabolism. This is often mediated by proteins containing Fe-S clusters (Lill, 2009; Rouault, 2015; Fuss et al., 2015). For instance, the large subunit of the eukaryotic DNA primase (PRIM2) requires an intact Fe-S cluster to bind DNA and synthesize short RNA primers at the onset of DNA replication; in addition, all B family DNA polymerases, such as DNA pol ε and δ, display a cysteine-rich domain that coordinates Fe-S clusters necessary for polymerization of nascent strands (Netz et al., 2012; Klinge et al., 2007; Burgers and Kunkel, 2017). Finally, many DNA helicases feature a conserved Fe-S cluster that is directly involved in the opening of the double helix to allow nucleotide excision repair (XPD), G-quadruplex-structure resolution (FANCJ), DNA double-strand break repair (DNA2), and telomere duplication (RTEL1), indicating an essential role for iron-containing proteins in the maintenance of genome stability (Rudolf et al., 2006; Pokharel and Campbell, 2012; Uringa et al., 2011). Accordingly, mutations of amino acids that bind Fe-S clusters (as it occurs in XPD or FANCJ) or loss-of-function mutations of proteins like Frataxin (part of the cytosolic/mitochondrial Fe-S cluster assembly machinery, ISC) or MMS19 (key component of the CIA complex that mediates the incorporation of Fe-S cluster into ERCC2/XPD, FANCJ and RTEL1) have been associated to the development of severe genetic disorders characterized by defects in DNA replication and repair, such as trichothiodystrophy, Fanconi anemia, and Friedreich's ataxia (Elledge et al., 1992; Gari et al., 2012; Stehling et al., 2012; Stehling and Lill, 2013). On the other hand, intracellular iron concentrations must be carefully controlled, as excessive iron can catalyze the production of reactive oxygen species (ROS) via Fenton reaction with consequent oxidative damage of proteins, lipids, and DNA (Galaris et al., 2019). Thus, balancing intracellular iron levels is fundamental to sustain DNA metabolism and avoid potential harmful effects.

Little is known about the mechanisms that coordinate intracellular iron levels with DNA transactions in the nucleus. Low iron levels have been shown to induce cell-cycle arrest in G1

due to a p53-dependent decrease in cyclin expression and CDK activity (Yu et al., 2007; Zhang, 2014). This might explain the well-known antitumor activity of iron chelating agents (Torti et al., 2018). However, how cells cope with unbalanced iron levels, specifically during active DNA replication in S phase when the double-stranded DNA (dsDNA) molecule is unwound and exposed to dangerous oxidative reactions, is unknown. Understanding the regulation of these processes might unveil new mechanisms involved in control of genome stability and potentially reveal specific vulnerabilities of cancer cells that are strictly addicted to high iron uptake and storage (Torti et al., 2018).

The nuclear receptor co-activator 4 (NCOA4) gene was initially identified in papillary thyroid carcinoma (PTC) as a fusion partner of the receptor tyrosine kinase RET gene (Santoro et al., 1994). More recently, a seminal work from Mancias and co-workers identified NCOA4 as a cargo receptor mediating autophagic degradation of ferritin. Ferritin is a multiprotein nanocage composed of 24 subunits of heavy (FTH1) and light (FTL) chains that stores iron in the cytosol to prevent spurious Fenton reactions and to serve as a source of iron when its intracellular concentration decreases (Mancias et al., 2014; Dowdle et al., 2014). NCOA4 selectively binds to a conserved C-terminal FTH1 domain and to autophagy-related proteins (ATGs), such as GABARAP and GABARAPL1, to deliver iron-laden ferritin to autophagosomes and promote iron release via lysosomal degradation in a process known as ferritinophagy (Mancias et al., 2014, 2015). Iron deficiency triggers NCOA4-mediated ferritinophagy to maintain stable intracellular iron levels and sustain essential iron-dependent metabolic processes. On the other hand, in iron repleted conditions NCOA4 binds iron and is recognized by the E3 ligase HERC2. HERC2-dependent NCOA4 polyubiquitination results in its proteasomal degradation and block of ferritin autophagy (Mancias et al., 2015). Importantly, lack of NCOA4-mediated ferritinophagy *in vivo* impairs systemic iron homeostasis, inducing ferritin accumulation in several organs such as liver, spleen, and duodenum and leading to increased susceptibility to anemia (Bellelli et al., 2016; Santana-Codina et al., 2019; Nai et al., 2021).

We identified NCOA4 as a novel interactor of MCM7, a component of the MCM2-7 helicase complex that provides the essential unwinding activity during eukaryotic DNA replication, as part of the so-called CMG (CDC45-MCM2/7-GINS1/4) complex (Bell and Labib, 2016). By binding to MCM7, NCOA4 prevents inappropriate DNA replication origin activation to avoid replication stress and genomic instability (Bellelli et al., 2014). However, it remains to be established when such NCOA4 activity is required and how it is regulated.

Here, we show that iron deficiency triggers nuclear NCOA4 stabilization and binding to the MCM2-7 complex, resulting in inhibition of DNA replication origin activation. Upon NCOA4 ablation, cells become insensitive to iron depletion and undergo inappropriate DNA synthesis, which generates replication stress and compromises cell proliferation and viability. Such mechanism is fundamental *in vivo* to support intense cell proliferation as it normally occurs during tissue regeneration.

RESULTS

Reduced iron bioavailability impairs cell-cycle progression and DNA replication

To verify whether variation in intracellular iron levels affected cell proliferation and DNA replication, we treated asynchronous HeLa cells with the iron chelator deferoxamine (DFO) mesylate and analyzed cell-cycle progression by propidium iodide (PI) staining and flow cytometry. As expected, iron chelation caused cell-cycle arrest, with more than 90% of cells blocked in G1 phase after 16 h of DFO treatment (Figure 1A). Indeed, the expression of the S-phase-specific cyclin E was already reduced after 10 h of DFO treatment (Figures 1B and S1A). Thus, in agreement with previous reports (Yu et al., 2007; Zhang, 2014), low iron availability impairs cell-cycle progression by preventing S-phase entry. DFO treatment was also associated with signs of DNA damage, as shown by increased phosphorylation of Chk1 on Ser345 (Figures 1B and S1A) and histone H2AX on Ser139 (a modification also known as γH2AX) (Figure 1C) (Zeman and Cimprich, 2014; Técher et al., 2017). Interestingly, cells with the strongest γH2AX signal showed a DNA content between 2N and 4N, characteristic of cells in S phase (Figure 1D), suggesting that the absence of iron induced DNA damage particularly during DNA replication (Jackson and Bartek, 2009).

To further investigate how low iron levels affects DNA replication, we analyzed the replication dynamics of HeLa cells exposed to DFO for 2 h, using the DNA fiber stretching assay (Bellelli et al., 2014). In DFO-treated cells, we observed a strong reduction of labeled fibers compared with control, confirming that iron deprivation reduces S-phase entry (data not shown). Moreover, in DFO-treated cells, the few labeled fibers showed a strong reduction in the mean replication fork rate compared with those from untreated cells (0.600 ± 0.029 versus 0.915 ± 0.03 Kb/min) (Figure 1E). DFO treatment also promoted accumulation of asymmetric forks as well as reduction of inter-origin distance (IOD), revealing the occurrence of fork stalling and activation of dormant DNA replication origins (Figures 1F and 1G). Reduced fork speed, reduced IOD, and increased fork asymmetry are hallmarks of replication stress (Zeman and Cimprich, 2014; Técher et al., 2017).

To specifically analyze DNA replicating cells, we synchronized HeLa cells at the beginning of the S phase by double thymidine (Thy) block. Strikingly, when released in DFO-conditioned medium, Thy-arrested cells were unable to efficiently resume DNA synthesis, showing a delayed progression through S phase, when compared with untreated cells, probably due to the accumulation of stalled DNA replication forks (Figure 1H).

To confirm that iron depletion induced stalling of ongoing replication forks and required activation of dormant origins, we evaluated sensitivity of HeLa cells to low iron in conditions of minimal licensing (reduced number of dormant origins) (Ibarra et al., 2008). We reduced MCM2 protein abundance by RNA silencing and evaluated cell viability and proliferation upon cell treatment with DFO (Figure S1B). In accordance with previous data (Ibarra et al., 2008), MCM2 down-regulation only slightly reduced cell proliferation (Figure S1C), likely due to the timely repair of damaged replication forks (Ibarra et al., 2008). Of note, MCM2-depleted cells became hypersensitive to DFO (6 h), displaying

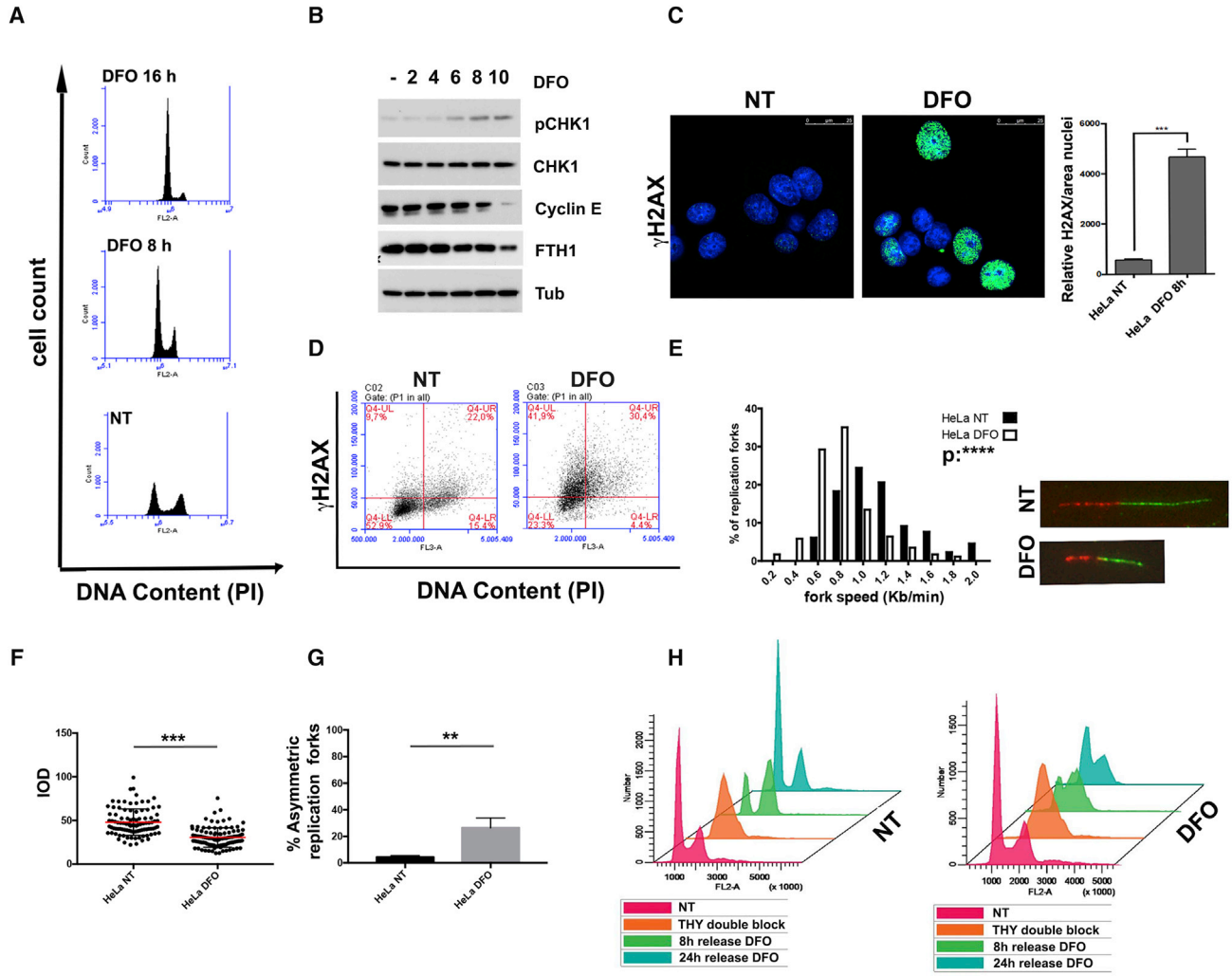

Figure 1. Iron is fundamental for cell-cycle progression and DNA replication

(A) Cytofluorimetric analysis of asynchronous HeLa cells treated with vehicle (NT) or 100 μM deferoxamine (DFO) for 8 and 16 h and stained with propidium iodide.

(B) Western blot analysis of cyclin E (cyclin E), ferritin heavy chain (FTH1), Chk1, and phospho-Chk1 (pChk1) of DFO-treated HeLa cells harvested at the indicated time points. Tubulin (Tub) was used as loading control.

(C) Left: representative images of confocal immunofluorescent analysis of γH2AX staining in HeLa cells treated with vehicle (NT) or with 100 μM DFO (DFO) for 8 h. Scale bar, 25 μm. Right: relative quantification of γH2AX immunofluorescence intensity per nuclei.

(D) Flow cytometry analysis of HeLa cells treated with vehicle (NT) or 100 μM DFO (DFO) for 16 h and stained with γH2AX antibody and propidium iodide.

(E) DNA fiber stretching analysis of asynchronous HeLa cells treated with vehicle (NT) or with 100 μM DFO (DFO) and pulse labeled after 2 h of treatment with CldU and IdU. Left: bar graph represents the distribution of replication fork speed (Kb/min) of HeLa cells in normal (NT) or iron-depleted (DFO) conditions. A total of 271 (NT) and 258 (DFO) fibers were analyzed. Right: representative images of DNA fiber stretching of cells grown in not treated (NT) or DFO-containing complete medium. Two-way ANOVA was performed by comparing the mean of frequency of fork rate between untreated (NT) and DFO-treated HeLa cells. ***$p > 0.0001$.

(F) Graph showing mean inter-origin distance (IOD) of vehicle- or 100 μM DFO-treated (2 h) HeLa cells sequentially labeled with CldU and IdU.

(G) Percentages of asymmetric replication forks in HeLa cells treated with vehicle (NT) or with 100 μM DFO (DFO). Fork asymmetry is considered when ratio between the two DNA strands is less than 0.6.

(H) Cell-cycle analysis of HeLa cells synchronized at the beginning of S phase by double thymidine block and released in not treated (NT) (left panel) or in DFO-containing complete medium (right panel). t test **$p < 0.01$; ***$p < 0.001$.

a progressive reduction in cell proliferation compared with untreated cells (35.3% after 24 h and 62% after 48 h) (Figures S1C and S1D). In contrast, DFO only slightly affected the proliferation of cells transfected with a control siRNA (siCTR). Indeed, siCTR cells showed a reduction of 25% after 24 h and almost completely resumed proliferation at 48 h (Figures S1C and S1D). Furthermore, siMCM2 cells also displayed a reduction of colony-forming ability compared with control cells (Figures S1E and S1F). These results likely reflected the inability of cells to resume DNA replication, upon iron chelation, in conditions of "limited licensing" and insufficient backup of dormant origins.

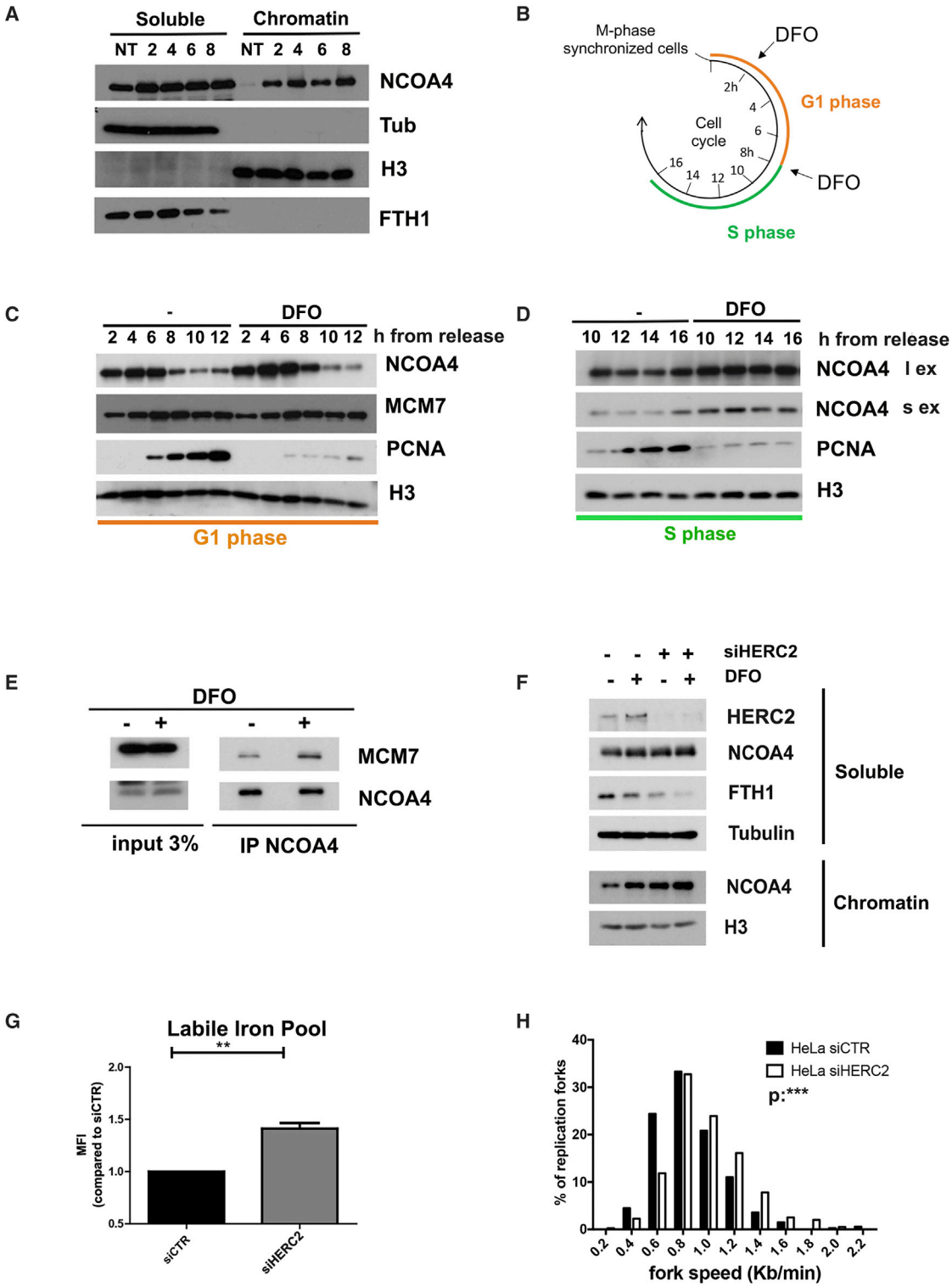

Figure 2. Intracellular iron levels control NCOA4 nuclear function

(A) Western blot analysis of NCOA4 and FTH1 proteins in soluble and chromatin fractions from DFO-treated HeLa cells harvested at the indicated time points. Tub and histone H3 (H3) were used as loading control.

(B) Schematic representation of DFO treatment at specific time points of the cell cycle. HeLa cells were initially synchronized in M phase by Nocodazole arrest and released in complete medium. After 2 (orange line) or 8 (green line) hours cells were then treated with DFO and harvested at the indicated time points.

(legend continued on next page)

All together, these data indicate that decreased iron availability might represent an important source of replicative stress during cellular proliferation.

Iron deficiency promotes NCOA4 nuclear stabilization and binding to unfired DNA replication origins

The mechanisms that allow cells to finely "tune" DNA replication to intracellular iron bioavailability are largely unknown. We focused on the iron-binding NCOA4 protein, which controls intracellular iron levels, by promoting ferritin degradation, as well as DNA replication, by negatively regulating the MCM2-7 helicase (Mancias et al., 2014; Dowdle et al., 2014; Bellelli et al., 2014). First, we monitored NCOA4 protein levels, upon iron depletion, in both soluble (cytosol and nucleoplasm) and chromatin-bound cell fractions (Figure S2A). In agreement with previous studies (Mancias et al., 2014, 2015; Bellelli et al., 2016), decreased iron concentrations induced not only a rapid stabilization of cytosolic NCOA4 and, consequently, ferritin degradation but also an increase of chromatin-bound NCOA4 (Figures 2A and S2B). Accordingly, treatment of the chromatin-bound protein fraction with DNase completely released NCOA4 in the supernatant (Figure S2B). Moreover, impairing nuclear transport via inhibition of α/β importin reduced NCOA4 accumulation into nucleus both in untreated as well as in iron-depleted conditions (Figure S2C), indicating that NCOA4 migration in the nucleus increased after iron chelation.

We have previously shown that NCOA4 chromatin levels change during cell-cycle peaking in late G1 and progressively decrease during S phase (Bellelli et al., 2014). Thus, to exclude that NCOA4 enrichment on chromatin upon DFO treatment was merely secondary to the cell-cycle arrest (Figure 1A), we monitored chromatin levels of NCOA4 in synchronized HeLa cells, treated with DFO in G1 or S phase (Figure 2B). Chromatin-bound NCOA4 levels increased in G1 phase up to 6 h from nocodazole release and then started decreasing upon entry in S phase (8 h from nocodazole release) (Figures 2C and S2D) (Bellelli et al., 2014). Addition of DFO in G1 promoted a further increase of NCOA4 recruitment to chromatin (Figures 2C and S2D), parallel to G1 arrest and delayed S-phase entry as shown by reduced levels of D and E cyclins (Figure S2E) and of proliferating cell nuclear antigen (PCNA) chromatin binding (Figure 2C). In S phase (8 h from nocodazole release), when thousands of replication origins are typically activated, NCOA4 binding to chromatin was decreased (Figures 2D and S2F). Upon iron depletion, both NCOA4 loading onto chromatin and binding to MCM7 were increased, parallel to a strong decrease of PCNA, pointing to a NCOA4-dependent block of origin activation and S-phase arrest (Figures 2D, 2E, S2F, and S2G). Impairment of cyclin E down-regulation also indicated arrest in S phase (Figure S2H).

Under iron-depleted conditions, NCOA4 may increase its binding to MCM2-7 complexes located at unfired replication origins (to prevent their activation) or to active, but stalled, MCM2-7-associated replication forks (possibly to restrain polymerases-helicase uncoupling upon replication fork stalling). To discriminate between these two possibilities, we searched for NCOA4 enrichment at DFO-stalled replication forks by iPOND (isolation of proteins on nascent DNA) (Figure S3A, left panel) (Dungrawala and Cortez, 2015). In agreement with our previous findings, in unperturbed DNA replication, NCOA4 was excluded from both active replication forks (where PCNA levels are high) and newly replicated chromatin after a Thy chase (where PCNA levels are low) (Figure S3A, right panel) (Bellelli et al., 2014). Upon DFO treatment, NCOA4 was not detectable on nascent DNA, thus excluding its recruitment to stalled forks (Figure S3A, right panel). DFO-mediated fork stalling was confirmed by the recruitment of the Rad51 recombinase (Figure S3A, right panel) (Bhat and Cortez, 2018). Accordingly, we failed to co-immunoprecipitate NCOA4 with proteins localized at active replication forks, such as DNA polymerases or PCNA, under both untreated or DFO-treated conditions (Figures S3B, S3C, and S3D).

We then explored the mechanism mediating NCOA4 recruitment to chromatin in low-iron conditions. Mancias and coworkers showed that the ubiquitin ligase HERC2 promotes NCOA4 degradation in iron-repleted conditions (Mancias et al., 2015). Thus, we hypothesized that HERC2, by modulating NCOA4 stability, may be also involved in regulating NCOA4 nuclear function. As expected, upon transient silencing of HERC2 (siHERC2), NCOA4 levels increased in the soluble fraction and promoted ferritin degradation, as suggested by reduced FTH levels (Figure 2F, soluble fraction, and S3E), thereby inducing an increase of the labile iron pool (LIP), measured by calcein fluorescent assay (Figures 2G and S3F), and a decrease of transferrin receptor 1 (Figure S3G). In addition, HERC2 silencing also promoted an increase of chromatin-bound NCOA4 (Figure 2F, chromatin fraction); this was associated with an overall reduction of DNA replication as assessed by reduced BrdU or EdU incorporation (Figures S3H and S3I). As expected, the reduction of the number of active forks was associated with a compensatory increase in fork speed (Figure 2H).

(C) Western blot analysis of NCOA4, MCM7, PCNA, and H3 proteins extracted from the chromatin fraction of G1-phase cells treated or not with DFO after 2 h from nocodazole release, as described in (B) (orange line).
(D) Western blot analysis of NCOA4 (long and short exposure), PCNA, and H3 proteins extracted from the chromatin fraction of S-phase cells treated or not with DFO after 8 h from nocodazole release, as described in (B) (green line).
(E) Western blot analysis of total (input 3%) and immunoprecipitated (IP NCOA4) NCOA4 and MCM7 proteins from HeLa cells treated with vehicle (–) or 100 μM DFO (+) for 2 h.
(F) Western blot analysis of the indicated proteins from soluble (top panel) and chromatin (bottom panel) fractions of HeLa cells transfected with control siRNA (siCTR) or siRNA against the HERC2 ubiquitin ligase (siHERC2) and treated with vehicle (–) or 100 μM DFO (+) for 2 h.
(G) Flow cytometry analysis of labile iron pool (LIP) in HeLa cells transfected with siCTR or siHERC2. Cells were treated with calcein-Am, and then the average green fluorescence intensity was measured.
(H) Bar graph representing the distribution of replication fork speed (Kb/min) in HeLa cells transfected with siCTR or siHERC2. A total of at least 200 fibers for each condition were analyzed. **$p < 0.01$.

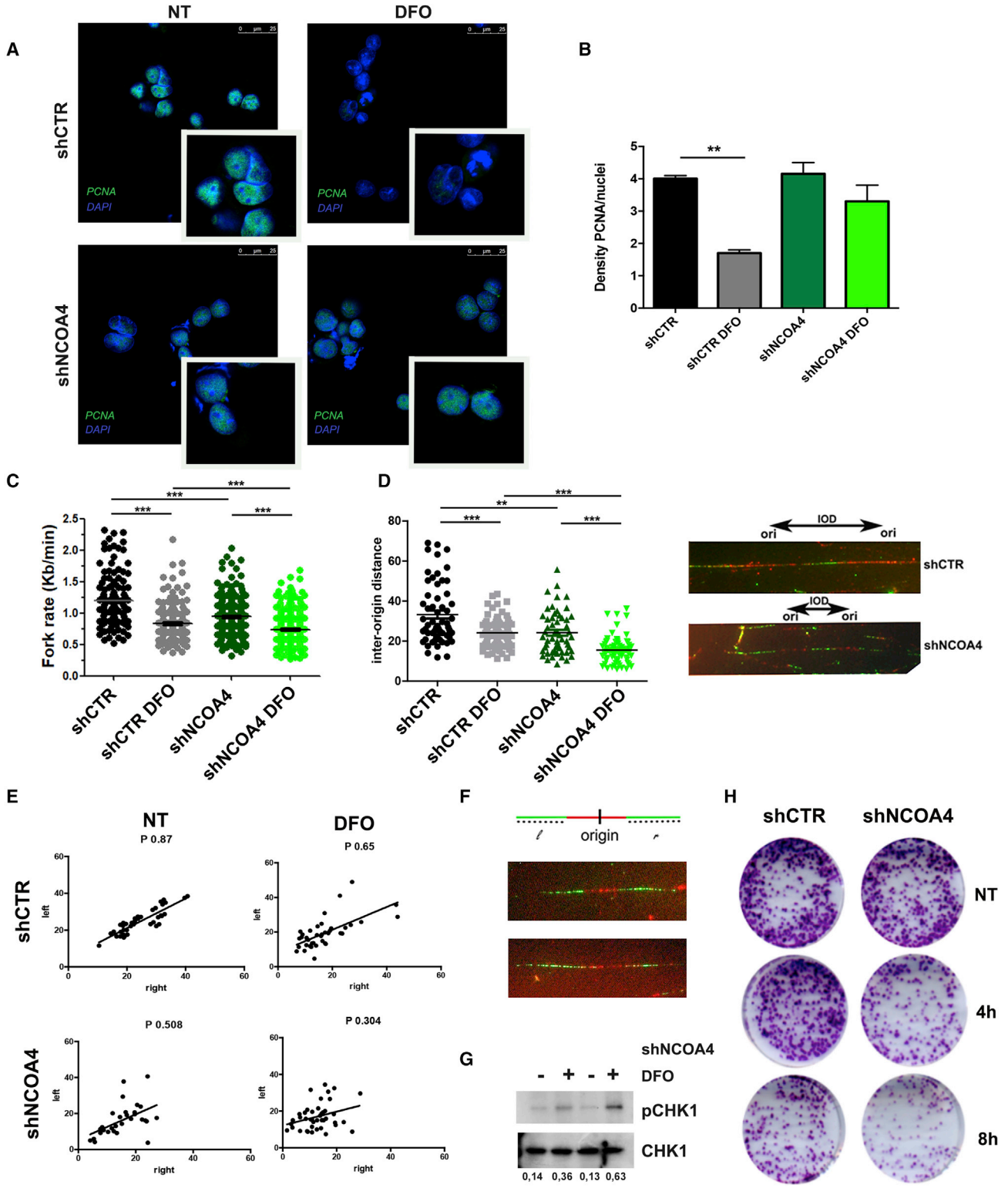

Figure 3. NCOA4 restrains new origins activation in iron depletion and prevents replication stress in low-iron conditions

(A) Representative images of confocal immunofluorescent analysis of PCNA foci in shCTR and shNCOA4 HeLa cells in basal (not treated [NT]) and iron-depleted (DFO) conditions (2 h).

(B) Bar graphs showing PCNA intensity staining of nuclei area of shCTR and shNCOA4 cells treated as in (A).

(legend continued on next page)

All together, these data indicate that iron-dependent NCOA4 turnover, mediated by the HERC2 ubiquitin ligase, modulates NCOA4 binding to chromatin and specifically to MCM2-7 in the context of unfired origins.

NCOA4 inhibits DNA replication origin activation and prevents replication stress in low-iron conditions

To verify whether NCOA4 binding to unfired DNA replication origins in low-iron conditions is functional to restrain their activation, we silenced NCOA4 in HeLa cells (shNCOA4 cells) and analyzed DNA replication. According to data reported in Figure 1, DFO treatment strongly reduced the density of PCNA foci (Figures 3A and 3B) and EdU incorporation (S4A and S4B) in control cells. In contrast, despite low iron levels, shNCOA4 cells maintained a significant level of DNA synthesis, as demonstrated by the higher number of PCNA foci (Figures 3A and 3B) and higher percentage of EdU-positive cells (Figures S4A and S4B) compared with control cells (shCTR cells). This indicates that NCOA4 absence causes unscheduled DNA replication origin firing in low iron. Of note, overexpression of NCOA4 in a tetracycline-regulated expression system (HeLa TREX NCOA4 cells; Figure S4C) reduced DNA synthesis, as demonstrated by decreased EdU incorporation (Figures S4D and S4E) and PCNA nuclear foci (Figures S4F and S4G), as well as cell proliferation (Figure S4H).

To investigate whether unscheduled DNA replication caused by NCOA4 loss generates replication stress, we silenced NCOA4 and analyzed replication fork rate, IOD, and fork asymmetry by DNA fiber stretching assay. In control cells, upon iron depletion, most origins are inactive; the few fired origins display a modest decrease of fork rate and IOD with a modest increase of fork asymmetry (Figures 3C–3F). Instead, in shNCOA4 cells, iron chelation induced a strong decrease in DNA replication fork rate and IOD with a remarkable increase in fork asymmetry (Figures 3C–3F). Moreover, already after 2 h of DFO treatment, shNCOA4 cells displayed a robust activation of DNA-damage response (DDR), as revealed by increased phosphorylation of Chk1 (Figure 3G) and H2AX (S4I and S4L), thus confirming the presence of replication stress. Replication stress and accumulation of DNA damage resulted in a reduction of colony-formation ability of shNCOA4 cells upon 4 or 8 h of DFO treatment compared with control cells (Figures 3H and S4M).

Overall, these data indicate that NCOA4 function is required to suppress activation of DNA replication origins in low-iron conditions, to prevent fork stalling and replication stress, and ensure genome stability and cellular viability.

Replication stress caused by NCOA4 knockdown is not caused by reduction of dNTPs and Fe-S cluster enzymes

In low-iron conditions, NCOA4 may also support DNA replication by promoting ferritin degradation and iron supply necessary for dNTP synthesis and for several replication enzymes' function. Therefore, to dissect the relative contribution of NCOA4 functions (DNA replication origin control versus ferritinophagy) upon iron deprivation, we verified whether the absence of NCOA4 affected LIP and "iron-dependent" enzymes both at the steady state and upon DFO treatment. NCOA4-depleted cells showed only a mild reduction in LIP, when compared with control cells, as assessed by calcein fluorescence staining (Figure 4A). In parallel, iron-responsive proteins, such as IRP2 and transferrin receptor 1 (TfR1) protein levels, were increased in shNCOA4 cells, likely to promote iron uptake from the extracellular environment to compensate reduced ferritinophagy (Figure 4B). Accordingly, even after 24 h of DFO treatment, deoxyadenosine triphosphate (dATP) levels were not significantly reduced in shNCOA4 cells compared with control cells, as demonstrated by a radioactive PCR-based assay (Figure 4C) (D'Angiolella et al., 2012). In addition, we did not detect any significant change in protein and RNA levels of the two major subunits of RRM, RRM1 and RRM2, upon NCOA4 silencing (Figures 4D and S5A). Similarly, the levels of several Fe-S cluster enzymes involved in DNA metabolism, such as DNA pol δ (Netz et al., 2012) (which is structurally stabilized by 4Fe-4S) and XPD and FANCJ helicases (Rudolf et al., 2006), were undistinguishable in shNCOA4 and control cells, both at the steady state and upon DFO treatment, decreasing in both cells only upon 24 h of treatment (Figure 4E). In line with these results, also the Fe-S-dependent conjugation of lipoic acid to the metabolic enzymes pyruvate dehydrogenase (PDH) and α-ketoglutarate dehydrogenase (KGDH) was not affected in NCOA4-depleted cells (Figure S5B). All together, these findings exclude that NCOA4 depletion causes major defects in Fe-S cluster assembly and Fe-S-cluster-dependent reactions.

To further demonstrate that NCOA4 deficiency was not inducing replication stress because of reduced dNTP production, we cultured cells in deoxynucleoside-supplemented culture media and evaluated replication dynamics (Figure 4F). In DFO-treated control cells, deoxynucleoside supplementation attenuated the mild reduction of fork speed, suggesting that, in this case, reduction of fork rate upon iron chelation is dependent on dNTP depletion. shNCOA4 cells showed lower fork-rate values when compared with control cells both in iron-repleted and -depleted conditions (Figures 3 and 4F); however, differently from what observed in control cells, addition of dNTPs did not

(C) Bar graphs showing replication fork speed (Kb/min) from shCTR and shNCOA4 HeLa cells treated with vehicle or 100 μM DFO for 2 h and then sequentially labeled with CldU and IdU.
(D) Left: bar graphs showing mean IOD of shCTR and shNCOA4 HeLa cells treated with vehicle or 100 μM DFO for 2 h and then sequentially labeled with CldU and IdU. Right: representative DNA fiber staining from shCTR and shNCOA4 cells treated with vehicle or DFO. IODs and origins (ori) are shown.
(E) Analysis of replication fork symmetry of shCTR and shNCOA4 cells treated with vehicle or 100 μM DFO for 2 h and then sequentially labeled with CldU and IdU. Lengths in Kb of left and right forks are plotted. P, Pearson coefficient.
(F) Representative pictures of symmetric (top panels) and asymmetric (bottom panels) replication forks. Left (l) and right (r) traits and ori are shown.
(G) Western blot analysis of the indicated proteins from chromatin fractions of shCTR and shNCOA4 HeLa cells released from nocodazole block for 8 h and then treated with vehicle or 100 μM DFO (2 h). On the bottom, densitometric analysis of pChK1 signal compared with total Chk1 protein.
(H) Representative pictures of colony-formation assays of shCTR and shNCOA4 HeLa cells treated with 1 mM DFO (4 or 8 h) and then grown for 12 days. Colonies were counted after crystal violet staining. *$p < 0.05$; **$p < 0.01$; ***$p < 0.001$.

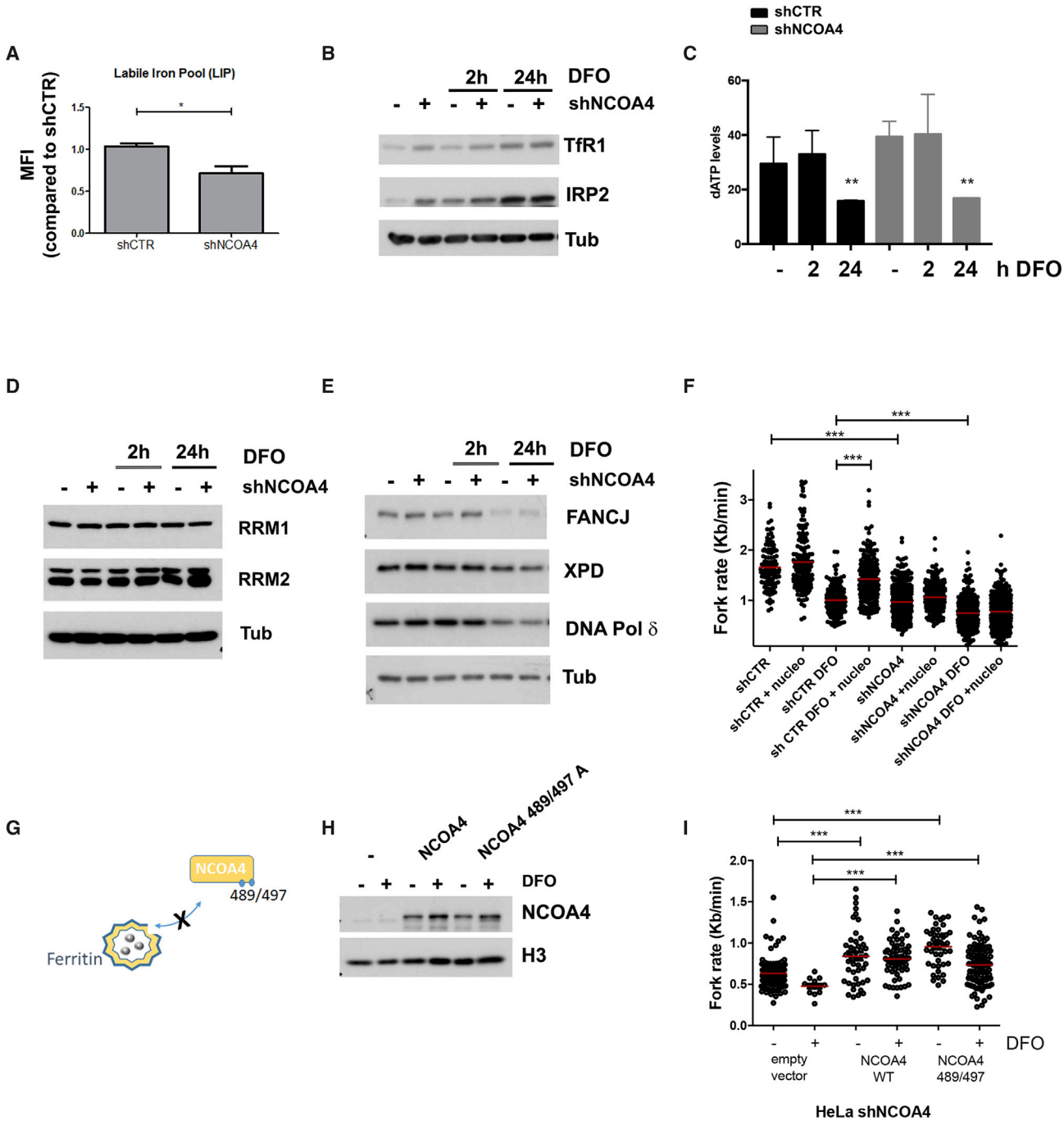

Figure 4. NCOA4 deficiency does not affect iron-dependent enzymes

(A) Flow cytometry analysis of LIP in shCTR and shNCOA4 cells. Cells were treated with calcein-AM and then incubated or not for 1 h with DFO. Mean fluorescence intensity (MFI) was calculated as mean of three different experiments and expressed as fold change with respect to shCTR mean fluorescence.

(B) Western blot analysis of the indicated iron responsive proteins (TfR1, transferrin receptor 1; IRP2, iron responsive protein 2) from shCTR and shNCOA4 cells treated for 2 or 24 h with vehicle or with DFO (100 μM). Tub was used as loading control.

(C) dATP levels in shCTR and shNCOA4 HeLa cells not treated (−) or treated with 100 μM DFO (+) for 2 or 24 h.

(D) Western blot analysis of ribonucleotide reductase subunits M1 and M2 (RRM1, ribonucleotide reductase catalytic subunit M1; RRM2, ribonucleotide reductase catalytic subunit M2) in shCTR and shNCOA4 cells treated as described in (B).

(E) Western blot analysis of the indicated Fe-S cluster proteins from shCTR and shNCOA4 cells treated as described in (B).

(F) Replication fork speed (Kb/min) of shCTR and shNCOA4 cells treated or not with 100 μM DFO for 2 h and then labeled with CldU and IdU. Cells were grown for 48 h in low or high (+ nucleo) deoxy-nucleoside medium and then incubated with halogenated nucleotides and processed for fiber stretching assay.

(legend continued on next page)

significantly increase their fork rate (Figure 4F). These data indicate that lack of dNTPs is not sufficient to explain the replication stress observed in the absence of NCOA4.

These findings suggested that the repression of replication origins by NCOA4 is key to prevent DNA damage in low-iron conditions. To further corroborate such a hypothesis, we evaluated the ability of NCOA4 489-497, an FTH-binding defective mutant, to rescue the replication stress observed in shNCOA4 cells (Mancias et al., 2015) (Figure 4G). NCOA4 489-497 retained the ability to bind to chromatin and to MCM7 (Figures S5C and 4H). Although, as expected, NCOA4 489-497 was unable to rescue ferritin degradation after DFO treatment of NCOA4-depleted cells (Figures S5D and S5E), it was still able to significantly ameliorate replication fork speed (Figure 4I).

All together, these data indicate that, in addition to its role in maintaining intracellular iron homeostasis through ferritinophagy, NCOA4 plays a crucial role in blocking inappropriate DNA replication in low-iron conditions, thus preventing replication stress caused by iron depletion.

Loss of NCOA4 leads to impaired intestinal regeneration and increased sensitivity to dextran sodium sulfate in mice

To evaluate the relevance of NCOA4 in coupling iron availability to DNA replication, we analyzed intestinal mucosa regeneration of NCOA4 wild-type (WT) (+/+) and null (−/−) mice after dextran sodium sulfate (DSS) treatment. Indeed, in tissue regeneration, DNA replication demands adequate iron availability. DSS induces a strong intestinal inflammation that causes extensive tissue damage with reduced crypts depth, ulceration, and bleeding (Chassaing et al., 2014). Upon DSS washout, intestinal mucosa is rapidly repaired by intense cell proliferation and tissue regeneration (Figure 5A). After 7 days, NCOA4+/+ and −/− animals were equally affected by DSS treatment, showing a similar reduction of colon length and of animal weight (Figures 5B, 5C, and S6A). However, while upon DSS wash out, NCOA4+/+ mice recovered, restoring normal colon length and body weight in ~6 days, NCOA4−/− mice failed to recover (Figures 5B and 5C). Consistently, after 6 days of DSS wash out, intestinal mucosa of NCOA4−/− mice featured alteration of tissue architecture and strong leucocytes infiltration, indicating an active inflammatory state likely due to impaired tissue repair (Figures 5D and S6B). In addition, after 6 days of wash out, colons from NCOA4−/− mice displayed a decreased number of mitotic (pH3-positive) cells (Figures 5D, S6B, and S6C) associated with a stronger positivity for phospho-Chk2 (marker of DNA damage) and cleaved caspase 3 (marker of apoptosis) compared with NCOA4+/+ animals (Figures 5D and S6D).

Intestinal regeneration is mainly sustained by stem cells, including crypt base columnar (CBC) and +4 (e.g., in position +4 from the crypt bottom) cells (Barker, 2014). Thus, we examined Lgr5 and BMI, expression markers of CBC and +4 stem cells, respectively, in both NCOA4+/+ and −/− mice intestines (Barker et al., 2007; Sangiorgi and Capecchi, 2008). DSS treatment induced a strong reduction of Lgr5 and BMI expression (Figure S6E) in both NCOA4+/+ and −/− animals, consistent with the extensive crypt loss (Figure S6B). However, during recovery from DSS, while control mice showed upregulation of Lgr5 and BMI, NCOA4−/− animals did not restore their expression, suggesting a significant proliferative defect of the stem cell compartment (Figure S6E). Interestingly, NCOA4+/+ and −/− mice displayed a reduction of transferrin saturation after 3 days of release from DSS treatment, presumably for intestinal bleeding and reduction of iron uptake. After 6 days, transferrin saturation improved in NCOA4+/+ animals, indicating tissue recovery from DSS treatment; on the contrary, no improvement was observed in NCOA4−/− mice, in accordance with an impairment of intestine regeneration in these animals. Moreover, after 6 days of DSS wash out, NCOA4+/+ crypt cells were able to grow in three-dimensional (3D) structures generating intestinal organoids (enteroids) (Figure S6G), whereas NCOA4−/− cells failed to form any enteroid (Figure S6F). After 10 days of DSS release, all NCOA4−/− mice died, while 80% of control animals survived (Figure 5E), pointing to a crucial role of NCOA4 function in maintaining integrity of the stem cell compartment and sustaining effective tissue regeneration *in vivo*.

To further corroborate such a model, we used intestinal organoids to model gut epithelial regeneration and directly studied the effect of iron chelation in this model (Figure 6A). NCOA4−/− crypts formed a slightly, but significantly, decreased number of organoids compared with NCOA4+/+ counterparts, suggesting a basal proliferation defect (Figures 6B and 6C). Addition of DFO for 24 h reduced NCOA4+/+ organoid development by around 50%, underlining the relevance of iron bioavailability in cell proliferation (Figures 6B and 6C). Noteworthy, crypts isolated from NCOA4−/− mice showed a higher sensitivity to iron depletion, being almost totally impaired in forming organoids upon DFO treatment (reduction of more than 90%). In agreement, iron chelation in well-established, multilobulated NCOA4+/+ enteroids promoted NCOA4 loading onto chromatin (Figure 6D), further suggesting a role for nuclear NCOA4 in restraining DNA replication in response to low iron levels.

Upon iron chelation, the inability of NCOA4−/− crypts to form organoids could be due to loss of NCOA4-mediated control of DNA replication. Thus, we analyzed DNA fibers isolated from organoids obtained from NCOA4+/+ and −/− mice after a short DFO treatment (6 h). In agreement with our previous data in HeLa cells, we observed a strong reduction of replication fork rate in NCOA4−/− organoids treated with DFO when compared with their WT counterpart (in NCOA4+/+ organoids: DFO/NT fork rate was 0.8; in NCOA4−/− organoids: DFO/NT fork rate was 0.4) (Figure 6E). Consistently, NCOA4−/− organoids showed signs of DNA damage after DFO treatment, as measured by nuclear γH2AX staining (Figure 6F), as well as an overall EdU incorporation (Figure 6G).

(G) Schematic representation of the NCOA4 489/497 mutant unable to bind ferritin.
(H) Western blot analysis of chromatin-bound NCOA4 WT and NCOA4 489/497 mutant from shNCOA4 cells transiently transfected with NCOA4 WT- and NCOA4 489/497-expressing vectors, treated with vehicle (−) or with 100 μM DFO (+) for 2 h and then sequentially labeled with CldU and IdU.
(I) Replication fork rate (kb/min) from shNCOA4 cells transiently transfected with NCOA4 WT or NCOA4 489/497 mutant and treated with vehicle or 100 μM DFO for 2 h. *$p < 0.05$; **$p < 0.01$; ***$p < 0.001$.

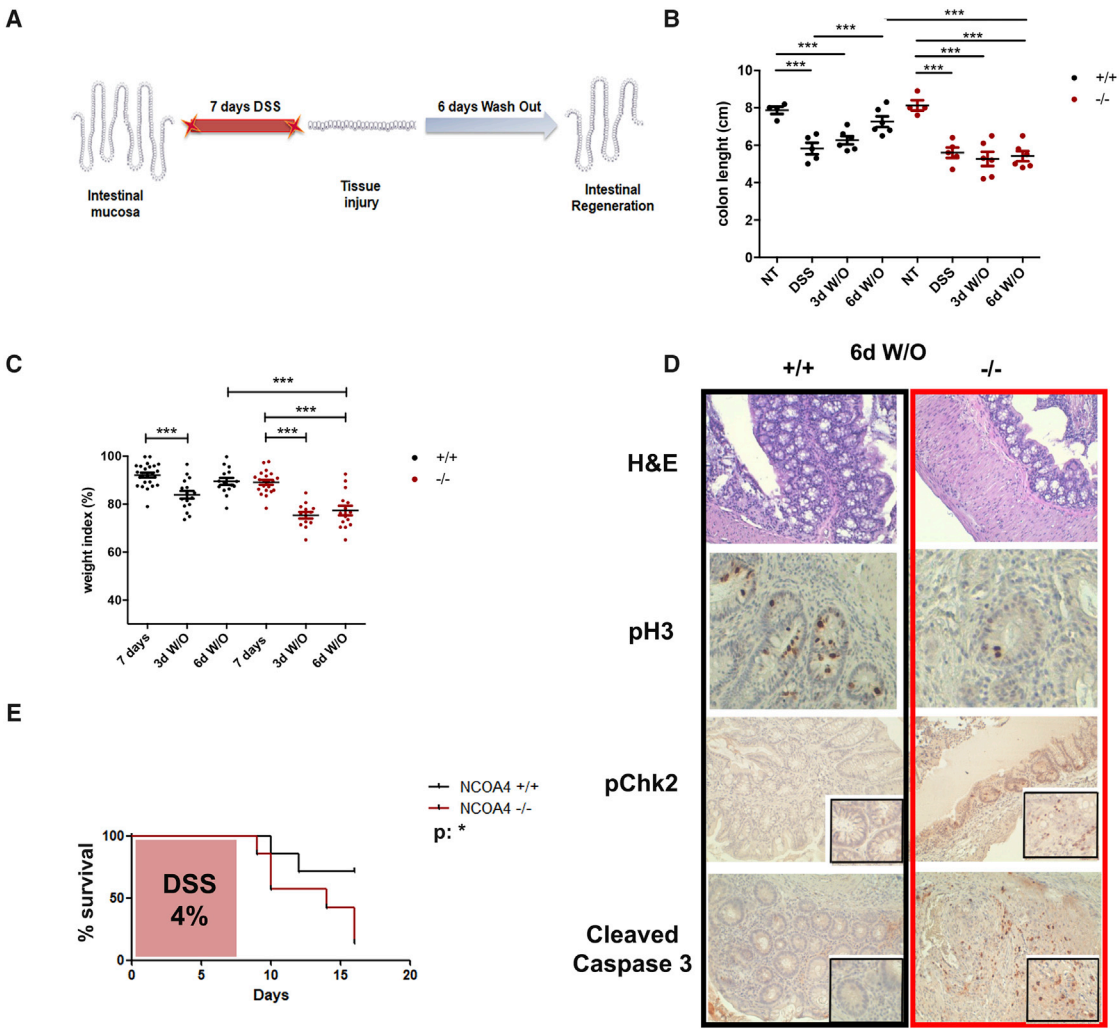

Figure 5. NCOA4-null mice are hypersensitive to DSS treatment and show impaired intestinal regeneration

(A) Scheme of the dextran sodium sulfate (DSS) treatment. Mice were treated with 4% DSS for 7 days to induce an intestinal injury. After 7 days, DSS was removed from drinking water to allow intestinal regeneration. Mice tissues were analyzed after DSS treatment (7 days) and after 3 and 6 days of wash/out (W/O).

(B) Colon length of NCOA4+/+ and −/− mice treated as described in (A). Between 4 and 6 animals for each group for each genotype: NT, DSS 7 days, 3 days W/O, and 6 days W/O were used.

(C) Body weight index of mice treated as described in (A). Values represent the average relative weight at sacrifice normalized to the weight measured the day before treatment started. Between 22 and 14 animals for each group for each genotype: NT, DSS 7 days, 3 days W/O, and 6 days W/O were used.

(D) Representative images of hematoxylin and eosin (H&E) and immunohistochemistry staining for pH3 (phospho histone H3), pChk2 (phospho Chk2), and cleaved caspase 3 of colon sections derived from NCOA4+/+ and −/− mice treated as described in (A).

(E) Kaplan-Meier plot showing survival of DSS-treated NCOA4+/+ and −/− mice. Ten animals for each genotype were used. *p < 0.05; **p < 0.01; ***p < 0.001.

All together, these data point to a fundamental role for NCOA4 in controlling DNA replication in low-iron conditions to maintain genome integrity and allow cellular proliferation and tissue regeneration.

DISCUSSION

Iron is a rate-limiting factor for cell proliferation because of its role in sustaining DNA replication, thus securing genome stability (Prá et al., 2012; Furukawa et al., 1992). Accordingly, previous work revealed a reprogrammed iron metabolism in proliferating cancer cells, featuring upregulation of critical genes involved in iron uptake, such as transferrin receptor (TFRC) (O'Donnell et al., 2006) and dimetal transporter 1 (DMT1) (Xue et al., 2016). On the contrary, reduction of cellular iron triggers a p53-mediated cell-cycle arrest (Yu et al., 2007; Zhang, 2014).

In this study, we observed that upon iron depletion, cells need the activation of dormant origins to overcome fork stalling and replication stress. Accordingly, depletion of dormant origins by MCM2 silencing (e.g., minimally licensed cells) sensitizes cells to iron chelation. Interestingly, a recent study found that inhibition of RRM activity, as it may occur during iron chelation, causes

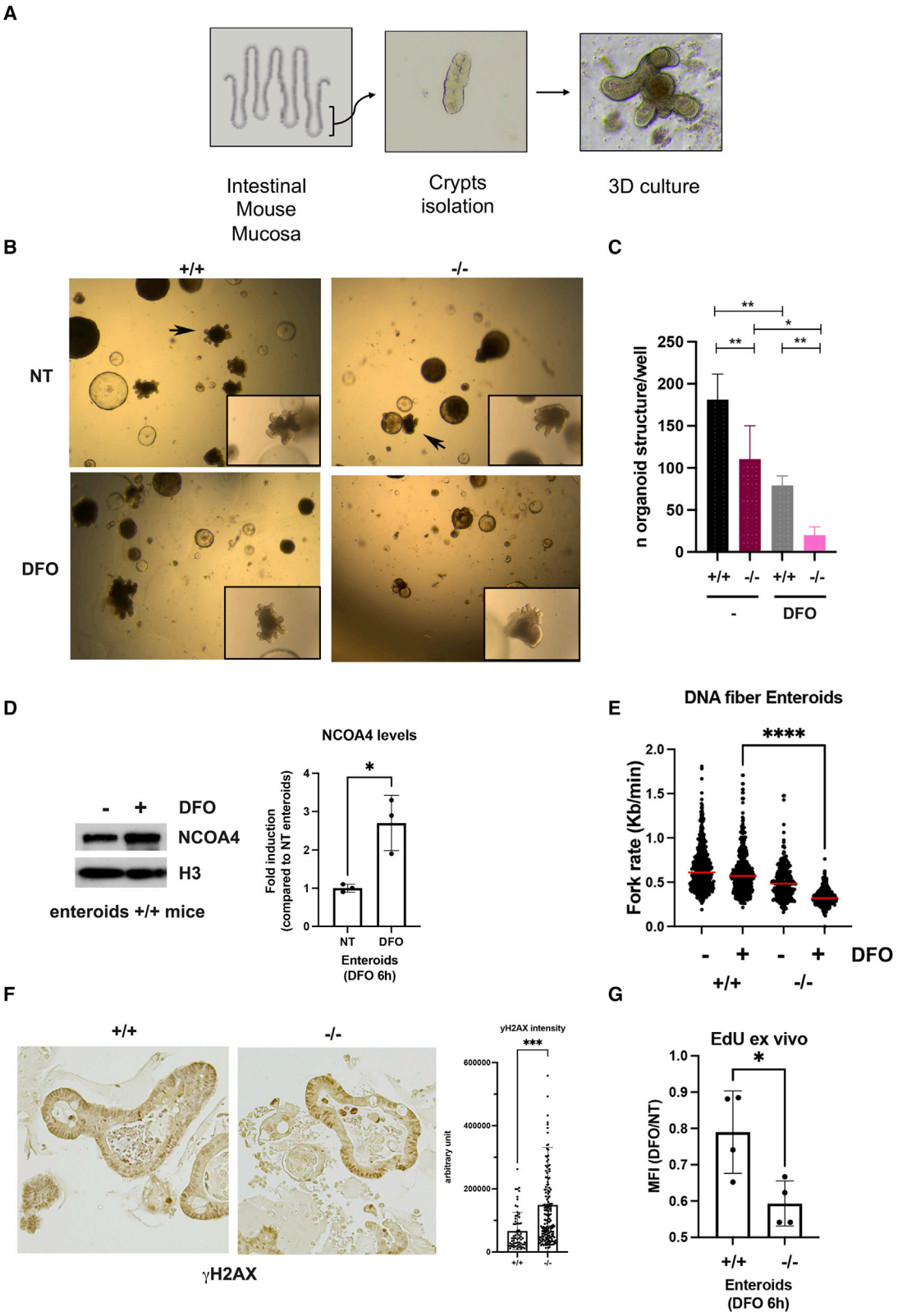

(legend on next page)

a redox imbalance and promotes replication protection complex (RPC) dissociation, thus slowing down replication forks (Somyajit et al., 2017).

NCOA4 is a negative regulator of DNA replication, able to hinder MCM2-7 helicase and block DNA replication origins. Indeed, its silencing in HeLa cells (this work) and genetic ablation in primary mouse fibroblasts (Bellelli et al., 2014) results in unscheduled replication origin activation, replication stress, and genome instability. On the other hand, NCOA4 is a central player in the control of iron homeostasis by promoting iron release from ferritin through ferritinophagy (Mancias et al., 2014). Moreover, NCOA4 levels are regulated by iron concentration, with iron-bound NCOA4 being recognized by the E3 ubiquitin ligase HERC2 and committed to proteasomal degradation (Mancias et al., 2015).

Based on this knowledge, we propose NCOA4 as a critical component of the cellular response that couples DNA replication to fluctuations of intracellular iron to safeguard genome stability. Here, we show that upon iron depletion, chromatin-bound NCOA4 levels increase as the consequence of reduced HERC2-mediated proteasomal degradation. In turn, chromatin-bound NCOA4 blocks DNA replication origins activation. When this control is lost, upon NCOA4 ablation, cells undergo inappropriate DNA replication and replication stress. Although it was feasible that NCOA4 could indirectly regulate DNA replication by sustaining intracellular iron levels, we show that NCOA4 depletion does not significantly affect Fe-S clusters and dNTP synthesis, probably because of cell compensation via upregulation of transferrin receptor. Thus, reduction of fork rate caused by NCOA4 depletion is not rescued by dNTP supply in DFO-treated cells. Moreover, a ferritinophagy-defective NCOA4 mutant largely maintained capability of restoring DNA replication control, preventing replication stress. We also posit that rapid NCOA4-mediated arrest of DNA replication needs to be associated with iron concentration restoration via ferritinophagy to fully maintain the iron-cell proliferation homeostasis. In this framework, it is critical that NCOA4 levels are then reduced when iron concentration is restored (Mancias et al., 2015). In agreement, overexpression of NCOA4 in iron-repleted conditions induces a decrease in BrdU incorporation and PCNA foci with consequent reduction of cell proliferation. However, it is possible that besides iron levels, other levels of NCOA4 regulation do exist, such as components of the DDR. For instance, HERC2 has been involved in DNA double-strand break repair as a target of the ATM kinase, potentially providing a link between NCOA4 and the DDR (Bekker-Jensen et al., 2010).

The relevance of the NCOA4-mediated circuit coupling iron levels to DNA replication is supported by the intestinal regeneration model. Impaired intestinal regeneration and extensive signs of DNA damage were observed in NCOA4−/− mice after DSS-induced colitis. We speculate that during the regenerative response after tissue injury, the absence of NCOA4 may cause unscheduled intestinal stem cell (ISC) proliferation regardless the higher iron demand, thus inducing dysregulated DNA replication, DNA damage, and cell death. In agreement, NCOA4−/− crypts displayed a marked decrease of their ability to form organoids *ex vivo*, especially upon iron chelation. This defect was paralleled by reduced rate of replication forks in NCOA4−/− enteroids treated with DFO compared with controls.

In conclusion, we propose that NCOA4 is a crucial player in the coordination between DNA replication and iron availability, preventing inappropriate DNA synthesis, replication stress, DNA damage and genome instability. Though we have shown the relevance of this function in tissue regeneration, we postulate that it may be important also in other highly proliferating cell contexts, for example neoplastic cells.

Limitations of the study

Although here we show that, in low-iron conditions, NCOA4 binds to inactive DNA replication origins, the genomic location and the nature of such origins remains to be identified. More specifically, it remains to be clarified whether NCOA4 binds to "dormant"

Figure 6. NCOA4−/− crypts generate fewer enteroids and show signs of replication stress in iron-depleted conditions *ex vivo*

(A) Schematic representation of the strategy used to establish mouse intestinal enteroids (small intestine). Crypts were isolated from mouse intestinal mucosa and then cultured into 3-dimensional matrix to generate differentiated enteroids.

(B) Representative images of intestinal enteroids derived from NCOA4+/+ and −/− mice observed at Leica microscope light (5× magnification) cultured for 7 days. Isolated crypts were cultured in Matrigel in the presence or not of DFO 100 μM. After 24 h, medium was replaced with complete medium. Arrows indicate well-differentiated enteroids after 7 days of culture.

(C) Bar graph depicting the mean number of enteroids per well derived from NCOA4+/+ and −/− mice after 7 days of culture as described in (B). Four independent experiments using 2 mice for each genotype were performed.

(D) Left: western blot analysis of NCOA4 chromatin-bound levels in NCOA4 WT-derived enteroids. Enteroids cultured for 7 days were treated with vehicle or DFO (100 μM) for 6 h and then purified from Matrigel. Chromatin-bound protein fraction was isolated from enteroids derived from 4 well by using CSK-triton buffer. Right: scatter plot depicting densitometric analysis of NCOA4 chromatin-bound protein extract derived from 7 day cultured enteroids treated or not with DFO. H3 was used as loading control. The ratio between DFO-treated and untreated enteroids of four independent experiments was calculated and plotted. Chromatin-bound proteins extracted from enteroids of 3 different mice were analyzed.

(E) Bar graphs showing replication fork speed (Kb/min) of DNA fibers from NCOA4+/+ and KO −/− enteroids treated with vehicle or 100 μM DFO. Seven day cultured entroids were treated for 6 h with 100 μM DFO and then sequentially labeled with CldU and IdU. Enteroids were purified from Matrigel, and then DNA fibers were isolated and processed for DNA stretching assay. A total of 400 fibers were analyzed, derived from enteroids from 3 different mice for each condition. t test ****$p < 0.0001$.

(F) Left: representative images of immunohistochemical analysis of γH2AX protein in paraffin-embedded organoids derived from NCOA4+/+ and −/− mice. Seven day cultured enteroids were treated with DFO for 6 h and subsequently processed for histological analysis. Right: scatter plot representing quantization of γH2AX signal per nucleus in paraffin-embedded enteroids treated as described above.

(G) Bar graph of EdU MFI derived from DFO-treated and untreated +/+ and −/− enteroids. Seven day cultured +/+ and −/− enteroids were treated for 6 h with 100 μM DFO and then labeled with EdU. Purified enteroids were dissociated, fixed, and processed for EdU analysis at cytofluorometer using the Click-iT kit. The ratio between MFI of DFO-treated and untreated enteroids was plotted. Each dot represents a different experiment. t test *$p < 0.05$.

replication origins and/or to late-replicating ones. Although in cells in culture, by using a ferritinophagy-deficient NCOA4 mutant, we could separate the role of NCOA4 in promoting ferritinophagy from that inhibiting DNA replication, we did not perform the same experiment in the animal-based intestinal regeneration model. Thus, it remains to be clarified which of the two NCOA4 functions is important for tissue regeneration in living animals. Finally, it remains to be addressed whether, besides intestine, NCOA4 is required also for regeneration of other tissues.

STAR★METHODS

Detailed methods are provided in the online version of this paper and include the following:

- KEY RESOURCES TABLE
- RESOURCE AVAILABILITY
  - Lead contact
  - Materials availability
  - Data and code availability
- EXPERIMENTAL MODEL AND SUBJECT DETAILS
  - Cell culture
  - Mouse model
- METHODS DETAILS
  - Cell synchronization
  - Cell fractionation and chromatin bound protein purification
  - Clonogenic survival assay
  - Flow cytometry
  - Calcein test
  - Immunofluorescence staining
  - Protein studies
  - RNA extraction and RT-PCR
  - Intestinal crypt isolation and enteroid culture
  - Histology
  - Transferrin saturation analysis
  - dATP concentration dosage
  - DNA fiber stretching
- QUANTIFICATION AND STATISTICAL ANALYSIS
  - Quantification
  - Statistics

SUPPLEMENTAL INFORMATION

Supplemental information can be found online at https://doi.org/10.1016/j.celrep.2022.111207.

ACKNOWLEDGMENTS

This work was supported by grants from the Fondazione Associazione Italiana Ricerca sul Cancro (grant IG 20793) and from Regione Campania (grant POR Campania FESR 2014–2020 "SATIN") for financial support. We thank Antonio D'Andrea for technical informatic assistance and Antonino Iaccarino for technical assistance in histological analysis. The graphical abstract was created using Biorender software (biorender.com).

AUTHOR CONTRIBUTIONS

F. Carlomagno, G.F., R.B., and M.S. designed the study and analyzed the data; F. Carlomagno, G.F., and R.B. wrote the manuscript; G.F., R.B., and F. Carrillo developed all methods for this study and performed lab experiments and *in vivo* experiments; M.C. and F.D. performed confocal immunofluorescence experiments; M.S. and M.C. revised the manuscript.

DECLARATION OF INTERESTS

All authors declare no conflict of interest.

Received: April 25, 2021
Revised: May 20, 2022
Accepted: July 22, 2022
Published: August 16, 2022

REFERENCES

Barker, N. (2014). Adult intestinal stem cells: critical drivers of epithelial homeostasis and regeneration. Nat. Rev. Mol. Cell Biol. *15*, 19–33. https://doi.org/10.1038/nrm3721.

Barker, N., van Es, J.H., Kuipers, J., Kujala, P., van den Born, M., Cozijnsen, M., Haegebarth, A., Korving, J., Begthel, H., Peters, P.J., and Clevers, H. (2007). Identification of stem cells in small intestine and colon by marker gene Lgr5. Nature *449*, 1003–1007. https://doi.org/10.1038/nature06196.

Bekker-Jensen, S., Rendtlew Danielsen, J., Fugger, K., Gromova, I., Nerstedt, A., Lukas, C., Bartek, J., Lukas, J., and Mailand, N. (2010). HERC2 coordinates ubiquitin-dependent assembly of DNA repair factors on damaged chromosomes. Nat. Cell Biol. *12*, 80–86. https://doi.org/10.1038/ncb2008.

Bell, S.P., and Labib, K. (2016). Chromosome duplication in Saccharomyces cerevisiae. Genetics *203*, 1027–1067. https://doi.org/10.1534/genetics.115.186452.

Bellelli, R., Federico, G., Matte', A., Colecchia, D., Iolascon, A., Chiariello, M., Santoro, M., De Franceschi, L., and Carlomagno, F. (2016). NCOA4 deficiency impairs systemic iron homeostasis. Cell Rep. *14*, 411–421. https://doi.org/10.1016/j.celrep.2015.12.065.

Bellelli, R., Castellone, M.D., Guida, T., Limongello, R., Dathan, N.A., Merolla, F., Cirafici, A.M., Affuso, A., Masai, H., Costanzo, V., et al. (2014). NCOA4 transcriptional coactivator inhibits activation of DNA replication origins. Mol. Cell *55*, 123–137. https://doi.org/10.1016/j.molcel.2014.04.031.

Bhat, K.P., and Cortez, D. (2018). RPA and RAD51: fork reversal, fork protection, and genome stability. Nat. Struct. Mol. Biol. *25*, 446–453. https://doi.org/10.1038/s41594-018-0075-z.

Burgers, P.M.J., and Kunkel, T.A. (2017). Eukaryotic DNA replication fork. Annu. Rev. Biochem. *86*, 417–438. https://doi.org/10.1146/annurev-biochem-061516-044709.

Chassaing, B., Aitken, J.D., Malleshappa, M., and Vijay-Kumar, M. (2014). Dextran sulfate sodium (DSS)-induced colitis in mice. Curr. Protoc. Immunol. *104*, 1–15. https://doi.org/10.1002/0471142735.im1525s104.

D'Angiolella, V., Donato, V., Forrester, F.M., Jeong, Y.T., Pellacani, C., Kudo, Y., Saraf, A., Florens, L., Washburn, M.P., and Pagano, M. (2012). Cyclin F-mediated degradation of ribonucleotide reductase M2 controls genome integrity and DNA repair. Cell *149*, 1023–1034. https://doi.org/10.1016/j.cell.2012.03.043.

Dowdle, W.E., Nyfeler, B., Nagel, J., Elling, R.A., Liu, S., Triantafellow, E., Menon, S., Wang, Z., Honda, A., Pardee, G., et al. (2014). Selective VPS34 inhibitor blocks autophagy and uncovers a role for NCOA4 in ferritin degradation and iron homeostasis in vivo. Nat. Cell Biol. *16*, 1069–1079. https://doi.org/10.1038/ncb3053. Epub 2014 Oct 19.

Dungrawala, H., and Cortez, D. (2015). Purification of proteins on newly synthesized DNA using iPOND. Methods Mol. Biol. *1228*, 123–131. https://doi.org/10.1007/978-1-4939-1680-1_10.

Elledge, S.J., Zhou, Z., and Allen, J.B. (1992). Ribonucleotide reductase: regulation, regulation, regulation. Trends Biochem. Sci. *17*, 119–123. https://doi.org/10.1016/0968-0004(92)90249-9.

Furukawa, T., Naitoh, Y., Kohno, H., Tokunaga, R., and Taketani, S. (1992). Iron deprivation decreases ribonucleotide reductase activity and DNA synthesis. Life Sci. *50*, 2059–2065. https://doi.org/10.1016/0024-3205(92)90572-7.

Fuss, J.O., Tsai, C.L., Ishida, J.P., and Tainer, J.A. (2015). Emerging critical roles of Fe-S clusters in DNA replication and repair. Biochim. Biophys. Acta *1853*, 1253–1271. https://doi.org/10.1016/j.bbamcr.2015.01.018.

Galaris, D., Barbouti, A., and Pantopoulos, K. (2019). Iron homeostasis and oxidative stress: an intimate relationship. Biochim. Biophys. Acta Mol. Cell Res. *1866*, 118535. https://doi.org/10.1016/j.bbamcr.2019.118535.

Gari, K., León Ortiz, A.M., Borel, V., Flynn, H., Skehel, J.M., and Boulton, S.J. (2012). MMS19 links cytoplasmic iron-sulfur cluster assembly to DNA metabolism. Science *337*, 243–245. https://doi.org/10.1126/science.1219664.

Ibarra, A., Schwob, E., and Méndez, J. (2008). Excess MCM proteins protect human cells from replicative stress by licensing backup origins of replication. Proc. Natl. Acad. Sci. USA *105*, 8956–8961. https://doi.org/10.1073/pnas.0803978105.

Jackson, S.P., and Bartek, J. (2009). The DNA-damage response in human biology and disease. Nature *461*, 1071–1078. https://doi.org/10.1038/nature08467.

Klinge, S., Hirst, J., Maman, J.D., Krude, T., and Pellegrini, L. (2007). An Fe-S domain of the eukaryotic primase is essential for RNA primer synthesis. Nat. Struct. Mol. Biol. *14*, 875–877. https://doi.org/10.1038/nsmb1288.

Lill, R. (2009). Function and biogenesis of iron-sulphur proteins. Nature *460*, 831–838. https://doi.org/10.1038/nature08301.

Mancias, J.D., Wang, X., Gygi, S.P., Harper, J.W., and Kimmelman, A.C. (2014). Quantitative proteomics identifies NCOA4 as the cargo receptor mediating ferritinophagy. Nature *509*, 105–109. https://doi.org/10.1038/nature13148.

Mancias, J.D., Pontano Vaites, L., Nissim, S., Biancur, D.E., Kim, A.J., Wang, X., Liu, Y., Goessling, W., Kimmelman, A.C., and Harper, J.W. (2015). Ferritinophagy via NCOA4 is required for erythropoiesis and is regulated by iron dependent HERC2-mediated proteolysis. Elife *4*, e10308. https://doi.org/10.7554/eLife.10308.

Miyoshi, H., and Stappenbeck, T.S. (2013). In vitro expansion and genetic modification of gastrointestinal stem cells in spheroid culture. Nat. Protoc. *8*, 2471–2482. https://doi.org/10.1038/nprot.2013.153.

Nai, A., Lidonnici, M.R., Federico, G., Pettinato, M., Olivari, V., Carrillo, F., Geninatti Crich, S., Ferrari, G., Camaschella, C., Silvestri, L., and Carlomagno, F. (2021). NCOA4-mediated ferritinophagy in macrophages is crucial to sustain erythropoiesis in mice. Haematologica *106*, 795–805. https://doi.org/10.3324/haematol.2019.241232.

Netz, D.J.A., Stith, C.M., Stümpfig, M., Köpf, G., Vogel, D., Genau, H.M., Stodola, J.L., Lill, R., Burgers, P.M.J., and Pierik, A.J. (2012). Eukaryotic DNA polymerases require an iron–sulfur cluster for the formation of active complexes. Nat. Chem. Biol. *8*, 125–132. https://doi.org/10.1038/nchembio.721.

O'Donnell, K.A., Yu, D., Zeller, K.I., Kim, J.W., Racke, F., Thomas-Tikhonenko, A., and Dang, C.V. (2006). Activation of transferrin receptor 1 by c-Myc enhances cellular proliferation and tumorigenesis. Mol. Cell. Biol. *26*, 2373–2386. https://doi.org/10.1128/MCB.26.6.2373-2386.2006.

Pokharel, S., and Campbell, J.L. (2012). Cross talk between the nuclease and helicase activities of Dna2: role of an essential Fe-S cluster domain. Nucleic Acids Res. *40*, 7821–7830. https://doi.org/10.1093/nar/gks534.

Prá, D., Franke, S.I.R., Henriques, J.A.P., and Fenech, M. (2012). Iron and genome stability: an update. Mutat. Res. *733*, 92–99. https://doi.org/10.1016/j.mrfmmm.2012.02.001.

Rouault, T.A. (2015). Mammalian iron-sulphur proteins: novel insights into biogenesis and function. Nat. Rev. Mol. Cell Biol. *16*, 45–55. https://doi.org/10.1038/nrm3909.

Rudolf, J., Makrantoni, V., Ingledew, W.J., Stark, M.J.R., and White, M.F. (2006). The DNA repair helicases XPD and FancJ have essential Fe-S domains. Mol. Cell *23*, 801–808. https://doi.org/10.1016/j.molcel.2006.07.019.

Sangiorgi, E., and Capecchi, M.R. (2008). Bmi1 is expressed in vivo in intestinal stem cells. Nat. Genet. *40*, 915–920. https://doi.org/10.1038/ng.165.

Santana-Codina, N., Gableske, S., Quiles del Rey, M., Małachowska, B., Jedrychowski, M.P., Biancur, D.E., Schmidt, P.J., Fleming, M.D., Fendler, W., Harper, J.W., et al. (2019). NCOA4 maintains murine erythropoiesis via cell autonomous and non-autonomous mechanisms. Haematologica *104*, 1342–1354. https://doi.org/10.3324/haematol.2018.204123.

Santoro, M., Dathan, N.A., Berlingieri, M.T., Bongarzone, I., Paulin, C., Grieco, M., Pierotti, M.A., Vecchio, G., and Fusco, A. (1994). Molecular characterization of RET/PTC3; a novel rearranged version of the RET proto-oncogene in a human thyroid papillary carcinoma. Oncogene *9*, 509–516.

Sato, T., Vries, R.G., Snippert, H.J., van de Wetering, M., Barker, N., Stange, D.E., van Es, J.H., Abo, A., Kujala, P., Peters, P.J., and Clevers, H. (2009). Single Lgr5 stem cells build crypt-villus structures in vitro without a mesenchymal niche. Nature *459*, 262–265. https://doi.org/10.1038/nature07935.

Somyajit, K., Gupta, R., Sedlackova, H., Neelsen, K.J., Ochs, F., Rask, M.B., Choudhary, C., and Lukas, J. (2017). Redox-sensitive alteration of replisome architecture safeguards genome integrity. Science *358*, 797–802. https://doi.org/10.1126/science.aao3172.

Stehling, O., Vashisht, A.A., Mascarenhas, J., Jonsson, Z.O., Sharma, T., Netz, D.J.A., Pierik, A.J., Wohlschlegel, J.A., and Lill, R. (2012). MMS19 assembles Fe-S proteins required for DNA metabolism and genomic integrity. Science *337*, 195–199. https://doi.org/10.1126/science.1219723.

Stehling, O., and Lill, R. (2013). The role of mitochondria in cellular iron-sulfur protein biogenesis: mechanisms, connected processes, and diseases. Cold Spring Harb. Perspect. Biol. *5*, a011312. https://doi.org/10.1101/cshperspect.a011312.

Técher, H., Koundrioukoff, S., Nicolas, A., and Debatisse, M. (2017). The impact of replication stress on replication dynamics and DNA damage in vertebrate cells. Nat. Rev. Genet. *18*, 535–550. https://doi.org/10.1038/nrg.2017.46.

Torti, S.V., Manz, D.H., Paul, B.T., Blanchette-Farra, N., and Torti, F.M. (2018). Iron and cancer. Annu. Rev. Nutr. *38*, 97–125. https://doi.org/10.1146/annurev-nutr-082117-051732.

Uringa, E.J., Youds, J.L., Lisaingo, K., Lansdorp, P.M., and Boulton, S.J. (2011). RTEL1: an essential helicase for telomere maintenance and the regulation of homologous recombination. Nucleic Acids Res. *39*, 1647–1655. https://doi.org/10.1093/nar/gkq1045.

van der Flier, L.G., van Gijn, M.E., Hatzis, P., Kujala, P., Haegebarth, A., Stange, D.E., Begthel, H., van den Born, M., Guryev, V., Oving, I., et al. (2009). Transcription factor achaete scute-like 2 controls intestinal stem cell fate. Cell *136*, 903–912. https://doi.org/10.1016/j.cell.2009.01.031.

Xue, X., Weisz, K., Triner, D., Xie, L., Attili, D., Pant, A., Győrffy, B., Zhan, M., Carter-Su, C., et al. (2016). Iron uptake via DMT1 integrates cell cycle with JAK-STAT3 signaling to promote colorectal tumorigenesis. Cell Metab. *24*, 447–461. https://doi.org/10.1016/j.cmet.2016.07.015.

Yu, Y., Kovacevic, Z., and Richardson, D.R. (2007). Tuning cell cycle regulation with an iron key. Cell Cycle *6*, 1982–1994. https://doi.org/10.4161/cc.6.16.4603.

Zeman, M.K., and Cimprich, K.A. (2014). Causes and consequences of replication stress. Nat. Cell Biol. *16*, 2–9. https://doi.org/10.1038/ncb2897.

Zhang, C. (2014). Essential functions of iron-requiring proteins in DNA replication, repair and cell cycle control. Protein Cell *5*, 750–760. https://doi.org/10.1007/s13238-014-0083-7.

STAR★METHODS

KEY RESOURCES TABLE

REAGENT or RESOURCE	SOURCE	IDENTIFIER
Antibodies		
Mouse Anti-cyclin B1	Santa Cruz Biotechnology	Cat#sc-594
Mouse anti-cyclin E	Santa Cruz Biotechnology	Cat#sc-247
Mouse anti-IRP2	Santa Cruz Biotechnology	Cat#sc-33682
Mouse anti-MCM7	Santa Cruz Biotechnology	Cat#sc-9966
Rabbit anti cyclin A	Santa Cruz Biotechnology	Cat#sc-751
Rabbit anti Histone H3	Santa Cruz Biotechnology	Cat# sc-10809
Rabbit horseradish peroxidase	BioRad	Cat#170-5046
Mouse horseradish peroxidase	BioRad	Cat#170-6516
Mouse Monoclonal anti-PCNA (PC10)	Calbiochem	Cat#NA03
Mouse monoclonal anti-Histone H3	Abcam	Cat#ab10799
Rabbit Anti-FTH1 (D1D4)	Cell signaling	Cat#43835
Rabbit Anti-Cleaved Caspase 3	Cell signaling	Cat#9661S
Rabbit Phospho Histone-3	Cell signaling	Cat#5701S
Rabbit Anti-pChK2	Novus Biologicals	Cat#NB100-92502
Mouse Anti-Transferrin Receptor 1	Life Technologies	Cat#136800
Mouse Anti-Tubulin	Sigma-Aldrich	Cat#T5168
Anti-lipoic acid	Millipore	Cat#437695
Rabbit Anti-HERC2	Bethyl	Cat#A301 905A
Rabbit anti-NCOA4	Bellelli et al., (2014)	N/A
Rabbit γH2AX	ThermoFisher Scientific	Cat#53-9865-82
rat anti-BrdU monoclonal antibody	Abcam	Cat#ab6326
mouse anti-BrdU monoclonal antibody B44	Becton Dickinson	Cay#347580
Rabbit Anti-Mouse IgG (H+L) Antibody, Alexa Fluor 546 Conjugated	Thermo Fisher	Cat#A11060
Goat Anti-Rat IgG (H+L) Antibody, Alexa Fluor 594 Conjugated	Thermo Fisher	Cat#A11007
Mouse anti-Myc	Santa Cruz Biotechnology	Cat#sc-40
Biotinylated goat anti-rabbit antibody	Vector Laboratories	Cat#BA-1000-1.5
Chemicals, peptides, and recombinant proteins		
EDTA-free Complete protease inhibitor cocktail	Roche	Cat#11873580001
EdU	Thermo Fisher Scientific	Cat#A10044
Biotin-Azide	Thermo Fisher Scientific	Cat#B10184
deferoxamine mesylate salt	Sigma-Aldrich	Cat#D9533
Streptavidin Sepharose high performance	GE Healthcare	Cat#17-5113-01
CuSO4	Sigma-Aldrich	Cat#PHR1477
Nocodazole	Sigma-Aldrich	Cat#M1404
Sodium L-Ascorbate	Sigma-Aldrich	Cat#A7631
Propidium Iodide	Sigma-Aldrich	Cat# P4170
Crystal violet	Sigma-Aldrich	Cat#C0775
DAPI	Sigma-Aldrich	Cat#10236276001
Cytidine	Sigma-Aldrich	Cat#4654
Thymidine	Sigma-Aldrich	Cat#T1865

(*Continued on next page*)

Continued

REAGENT or RESOURCE	SOURCE	IDENTIFIER
FOXP3 staining buffers	Milteny	Cat#130-093-142
Calcein AM	Sigma-Aldrich	Cat# 56496
TRIzol reagent	Invitrogen	Cat#15596026
M-MLV Reverse Transcriptase	ThermoFisher Scientific	Cat#28025021
SYBR green	Biorad	Cat#1725271
Matrigel	BD Bioscience	Cat#356231
Y-27632	Sigma Aldrich	Cat#Y0503
A8301	Tocris	Cat#2939
3,3'-Diaminobenzidine (DAB)	Sigma-Aldrich	Cat#D12384
[^{3}H] dTTP	Perkin Elmer	Cat#NET221A250UC
Whatman DE81 paper	GE Healthcare	Cat#3658-023
Klenow Fragment	ThermoFisher Scientific	Cat#EP0052
CldU	Sigma-Aldrich	Cat#C6891
IdU	Sigma-Aldrich	Cat#I7125
Doxicicline	Sigma-Aldrich	Cat#D9891
Cloroquine diphosphate	Fluka analytical	Cat#25745
Ferric Ammonium Citrate (FAC)	Sigma- Aldrich	Cat#D9891
Critical commercial assays		
Lipofectamine RNAiMAX	Thermo Fisher	Cat#13778150
FuGene	Promega	Cat#E2311
Click-iT™ EdU Alexa Fluor™ 488 Flow Cytometry Assay Kit	ThermoFisher Scientific	Cat#C10632
BrdU staining kit	Roche	Cat#11296736001
Experimental models: Cell lines		
HeLa cell lines	ATCC	ATCC® CCL2™
Experimental models: Organisms/strains		
NCOA4 −/− mice	Bellelli et al., (2014)	N/A
Oligonucleotides		
Silencer pre-Designed siRNA Negative Control	Ambion by Life Technologies	AM4641
Silencer pre-Designed siRNA HERC2	Ambion by Life Technologies	AM16704
Silencer Pre-designed siRNA Negative Control	Ambion by Life Technologies	4390843
Silencer Pre-designed siRNA MCM2	Ambion by Life Technologies	AM16708
Forward WT allele NCOA4 GTAGATTGGGTTAACAGTAAT	Bellelli et al. (2014)	N/A
Reverse WT allele NCOA4 TACATGCATATACAGAAAAT	Bellelli et al. (2014)	N/A
Forward KO allele NCOA4 TCGTCCTGCAGTTCATTCAG	Bellelli et al. (2014)	N/A
Reverse KO allele NCOA4 GATCGGCCATTGAACAAGAT	Bellelli et al. (2014)	N/A
M Lgr5 Forward, GACAATGCTCTCACAGAC	van der Flier et al. (2009)	N/A
m Lgr5 Reverse, GGAGTGGATTCTATTATTATGG	van der Flier et al. (2009)	N/A
m Bmi1 Forward, TATAACTGATGATGAGATAATAAGC	van der Flier et al. (2009)	N/A
m Bmi1 Reverse, CTGGAAAGTATTGGGTATGTC	van der Flier et al. (2009)	N/A
m GAPDH Forward, CATGGCCTTCCGTGTTCCTA	This Paper	N/A

(*Continued on next page*)

Continued

REAGENT or RESOURCE	SOURCE	IDENTIFIER
m GAPDH Reverse, ATGCCTGCTTCACCACCTTCT	This Paper	N/A
h TFRC Forward, ACCGGCACCATCAAGCT	This Paper	N/A
h TFRC Reverse, TGATCACGCCAGACTTTGC	This Paper	N/A
h RRM1 Forward, ACCAACCGCCCACAACTTT	D'Angiolella et al., 2012	N/A
h RRM1 Reverse, TGCCATTAGTCCCAGCAATGT	D'Angiolella et al., 2012	N/A
h RRM2 Forward, GTGGAGCGATTTAGCCAAGAA	D'Angiolella et al., 2012	N/A
h RRM2 Reverse, CACAAGGCATCGTTTCAATGG	D'Angiolella et al., 2012	N/A
h GAPDH Forward, GCCATCAATGACCCCTTCATT	This Paper	N/A
h GAPDH Reverse, TTGACGGTGCCATGGAATTT	This Paper	N/A
Mutagenesis NCOA4 489I→A, TGCTGATTCCTTCCAAGTCGCAA AGAACAGCCCCTTGTCG	This Paper	N/A
Mutagenesis NCOA4 497W→A, GCCCCTTGTCGGAGGCGCTTATC AGGCCCC	This Paper	N/A
Mutagenesis NCOA4 shRNA resistant TCAGCAGCTCTACTCGGCTTGGGCCAGTT	This Paper	N/A
Recombinant DNA		
pLKO.1-Puro	Sigma-Aldrich	SHC001
pLKO.1-Puro shNCOA4	Sigma-Aldrich	SHCLNDNM_005437
pcDNA^{TM}3.1/myc	ThermoFisher Scientific	V80020
pcDNA^{TM}3.1/myc NCOA4 489-497	This paper	N/A
pcDNA 6/TR (T-Rex System)	ThermoFisher Scientific	#K1020-01
pcDNA 4/To plus NCOA4	This paper	N/A
Software and algorithms		
Adobe Photoshop CC	Adobe	http://www.adobe.com/es/products/photoshop.html
ImageJ	NIH	https://imagej.nih.gov/ij/
GraphPad Prism 7	GraphPad	https://www.graphpad.com/

RESOURCE AVAILABILITY

Lead contact

Further information and requests for resources and reagents should be directed to and will be fulfilled by the lead contact, Francesca Carlomagno (francesca.carlomagno@unina.it).

Materials availability

This study did not generate new unique reagents.

Data and code availability

- Any data reported in the paper will be available upon request from the lead contact.
- This paper does not report original code.
- Any additional information required to reanalyze the data reported in this paper is available from the lead contact upon request.

EXPERIMENTAL MODEL AND SUBJECT DETAILS

Cell culture

HeLa cells were cultured in RPMI supplemented with 10% fetal bovine serum (FBS), 50 μg/mL penicillin-streptomycin, and 2 mM L-glutamine. To induce iron depletion, cells were incubated for 2 or 24 h with 100 μM deferoxamine mesylate salt (DFO; Sigma-Aldrich, #D9533).

Mouse model

Mice were maintained under specific pathogen-free conditions in the animal facility of the Dipartimento di Medicina Molecolare Biotecnologie Mediche (University of Naples Federico II). All studies were conducted in accordance with the Italian regulations for experiments involving animals (Minister approval 343/2019-PR). NCOA4 −/− mice displayed a systemic inactivation of murine NCOA4 gene, as described in Bellelli et al. (2014). The experimental procedure used for murine genetic screening was conducted as in Bellelli et al. (2014). In brief, 7-days-old mice were genotyped by extracting DNA from phalanx. Genotype was determined by PCR using two different primers couples to detect either WT or KO alleles listed in the key resource table. Experiments were conducted on 12-month-old mice. In each group females and males were equally represented.

METHODS DETAILS

Cell synchronization

Deoxynucleoside Supplemented Medium was obtained from ThermoFisher Scientific (#12571063). For M phase synchronization, HeLa cells were incubated with complete medium in the presence of 100 μg/mL Nocodazole (Sigma-Aldrich, #M1404). After 16 h, M phase cells were collected by shake-off, washed and released in complete or DFO-conditioned medium. For double thymidine block, cells were incubated for 12 h with 2 mM Thymidine (Sigma Aldrich, #T1865), released in Cytidine (Sigma-Aldrich, #4654) conditioned medium for 8 h and then incubated again with 2 mM Thymidine for 17 h before release in complete medium in the presence or not of DFO.

Cell fractionation and chromatin bound protein purification

Cells harvested from 3.5-cm dishes were washed with PBS and resuspended in CSK buffer (10 mM PIPES, 100 mM NaCl, 300 mM sucrose, 1 mM MgCl2, 1 mM ATP, 0.5% Triton X-100, protease inhibitor tablet (Roche). Lysates were incubated for 10 min on ice and then subjected to centrifugation at 3000 rpm for 5 min. Two fractions were obtained: the supernatant fraction representing the CSK-soluble fraction containing proteins localized in the cytosol and in the nucleosol, and the pellet representing the CSK-insoluble fraction containing chromatin bound proteins. The pellet was washed once with CSK buffer and then dissolved in SDS loading buffer (Bellelli et al., 2014).

Clonogenic survival assay

One x 10^3 cells were plated in 6-well plate and incubated for 4 or 8 h with 1 mM DFO. After DFO removal and wash, cells were left to grow for 12 days and colonies were then stained with a solution composed of Crystal violet in 20% Methanol, 10% Acid Acetic. After extensive washing with 20% Methanol and 10% Acid Acetic, colonies were counted.

Flow cytometry

For analysis of EdU incorporation, cells were treated with 10 μM EdU for 30 min, trypsinized and washed with PBS. EdU staining was performed by using the EdU Click-iT kit (ThermoFisher Scientific, #C10632), according to manufacturer's instructions. For analysis of cell cycle with Propidium Iodide, cells were initially fixed in 70% Ethanol at −20°C. After 24 h, cells were incubated with a staining solution containing 0.1% NP40 and Propidium Iodide. For γH2AX staining, cells were fixed and permeabilized using FOXP3 staining buffers (Milteny, #130-093-142.), subsequently incubated with a secondary Ab conjugated anti γH2AX (1:100; ThermoFisher Scientific, # 53-9865-82) for 1 h at 4°C and then analyzed by flow cytometry using an Accuri C6 apparatus. Collected data were finally analyzed using the Accuri C6 software.

Calcein test

To determine Labile Iron Pool, 2.5 × 10^5 cells were incubated for 20 min with Calcein AM (Sigma-Aldrich, # 56496) and washed twice with PBS. Cells were then left untreated or incubated with 1 mM DFO-conditioned medium for 1 h. Mean Fluorescence Intensity (MFI) of samples was analyzed by using Accuri C6 flow cytometer and the differences between MFI of DFO-treated and untreated sample were calculated.

Immunofluorescence staining

For indirect immunofluorescence, cells plated on 12 mm glass slides were fixed in Methanol 100% for 10 min at −20°C, permeabilized with 0.2% Triton X-100 (5 min on ice), and then incubated with the appropriate antibodies for 1 h at 4°C. Slides were then washed with PBS 1X and incubated with secondary antibodies for 30 min in the dark (Alexa Fluor anti-mouse #A32723 and anti-rabbit

#A32740). Cells were finally washed with PBS 1X, counterstained with DAPI (ThermoFisher Scientific, #P36962) and analyzed with a confocal fluorescence microscope Leica (DMI4000B) using the Las AF software. 5-Bromo-2′-deoxy-uridine Labeling and Detection Kit was used for BrdU staining (Roche #11296736001)

Protein studies

Cells were lysed in a buffer containing 50 mM N-2-hydroxyethylpiperazine-N′-2-ethanesulfonic acid pH 7.5), 1% (vol/vol) Triton X-100, 150 mM NaCl, 5 mM EGTA, 50 mM sodium fluoride, 20 mM sodium pyrophosphate, 1 mM sodium vanadate, 2 mM phenylmethylsulphonyl fluoride and 1 μg/mL aprotinin. Lysates were clarified by centrifugation at 10,000 × g for 30 min. Lysates containing comparable amounts of proteins, estimated by a modified Bradford assay (Bio-Rad, Munchen, Germany), were immunoprecipitated (1500 μg) with the required antibody or subjected (35 μg) to direct Western blotting. Immune complexes were detected with the enhanced chemiluminescence kit (Amersham Pharmacia Biotech, Little Chalfort, UK). Densitometric analysis of signal was performed using ImageQuant.

RNA extraction and RT-PCR

RNA was isolated from snap-frozen mouse colon samples by using TRIzol reagent (Invitrogen, #15596026). 2.5 μg of RNA was reverse-transcribed with M-MLV Reverse Transcriptase (ThermoFisher Scientific, # 28025021). qRT-PCR reactions were done in triplicate using SYBR green (Biorad, #1725271), and fold changes were calculated with the following formula: $2^{-\text{(sample 1 }\Delta\text{Ct} - \text{sample 2 }\Delta\text{Ct)}}$, where ΔCt is the difference between the amplification fluorescence threshold of the mRNA of interest and the mRNA of the GAPDH used as an internal reference. The sequence of the primers used for qPCR are listed in the key resources table.

Intestinal crypt isolation and enteroid culture

Intestinal crypts from NCOA4 null and wt mice were isolated following the protocol described in Sato et al. (2009) (Sato et al., 2009). Briefly, isolated small or large intestines, as indicated, were flushed with PBS, fragmented and digested with PBS containing EDTA (2 mM). The digestion content was filtered through a 70 μm pore cell strainer to obtain the crypt fraction and remove any residual villous material. To obtain enteroids, crypts were plated in Matrigel (BD Bioscience, #356231) drops in 24-multiwell plates and cultured in 1:1 advanced DMEM/F12 medium (Gibco, #12634010) plus 1% Glutamax (Gibco, #35050061), 1% HEPES (Gibco, #15630080), 1.25 mM N-acetylcysteine, and L-WRN conditioned medium (Miyoshi and Stappenbeck, 2013). The medium was changed every 2 days. At the first 4 days of culture, the Rho kinase inhibitors Y-27632 (Sigma-Aldrich, #Y0503) and A8301 (Tocris, #2939) were added to the culture medium.

Histology

Formalin-fixed, paraffin-embedded (FFPE) 5 μm thick colon sections were stained with H&E by conventional methods or deparaffinized and rehydrated by serial passages through xylene and alcohol (from 100% to 50%) for immunohistochemical (IHC) staining. In brief, colon sections were incubated with 3% H_2O_2 to block endogenous peroxidase and then antigen retrieval was performed by boiling sections in Citrate buffer. Colon sections were then blocked in BSA 1% in PBS for 30 min and incubated over/night with primary antibodies at 4°C. After PBS washing, sections were incubated for 30 min at room temperature with biotinylated goat anti-rabbit antibody (Vector Laboratories, Burlingame, CA, USA #BA-1000-1.5) and finally stained with 3,3′-Diaminobenzidine (DAB) (Sigma-Aldrich, #D12384) and visualized under Leica DMD108 microscope.

Transferrin saturation analysis

Transferrin saturation (ratio of serum iron and total iron binding capacity expressed as a percentage) was calculated using the Serum Iron/UIBC (Unsaturated Iron Binding Capacity) and the TIBC (Total Iron Binding Capacity) kits (Randox Laboratories Ltd.) according to manufacturer's instructions.

dATP concentration dosage

dATP pool determination in whole-cell extracts was carried out as previously described (D'Angiolella et al., 2012). Two x 10^5 cells were initially fixed for 5 min in 60% ice cold methanol. After methanol removal by centrifugation, samples were dissolved in deionized water. 10 μL of each sample were then incubated with 0.625 U Klenow Fragment (ThermoFisher Scientific, #EP0052), a specific set of primers and [^{3}H] dTTP (Perkin Elmer, #NET221A250UC). After incubation for 1 h at 37°C, reactions were spotted onto Whatman DE81 paper (GE Healthcare, #3658-023). Dried Whatman filters were then washed with 5% Na_2HPO_4 and rinsed with distilled H_2O and 100% EtOH. Finally, radioactivity was measured in a LS 6500 Multi-Purpose Scintillation Counter (Beckman Coulter TM) using 3.5 mL Optiphase HiSafe 3 (PerkinElmer) scintillation fluid. Data shown represent the percentage of dNTP incorporation compared to the positive control from each experiment.

DNA fiber stretching

The fiber stretching assay was performed as described in Bellelli et al. (2014). Briefly, cells were treated or not with DFO (100 μM) for 2 h and sequentially labelled with 10 μM CldU (Sigma-Aldrich, #C6891) and 100 μM IdU (Sigma Aldrich, #I7125) in presence of DFO. After trypsinization, cells were counted and resuspended in PBS at a concentration of 5 × 10^5/mL. 2.5 μL of cell suspension were then

lysed on the top of a microscope slide in 7.5 μL of a buffer containing 0.5% SDS in 200 mM Tris-HCL, pH 7.4, 50 mM EDTA. Slides were then tilted allowing a stream of DNA to move slowly toward the end of the slide and after drying were then fixed in methanol/acetic acid (3:1) for 15 min at R.T. After denaturation in HCl 2.5 M (45 min R.T.) slides were blocked in 1% BSA/PBS and incubated with rat anti-BrdU monoclonal antibody (1:1000 overnight; Abcam, # (ab6326) and mouse anti-BrdU monoclonal antibody (1:500 1 h R.T.; Becton Dickinson (B44), # 347580). Slides were then incubated with a mix of Alexa Fluor 488 rabbit anti-mouse (1:500 R.T.; Invitrogen, #A11029) and Alexa Fluor 594 goat anti-rat antibodies (1:500 R.T.; Invitrogen, #A11007) for 45 min and mounted in PBS/Glycerol 1:1. At least 1000 DNA fibers were analyzed in each experiment. In particular, DNA trait length values were measured via the ImageJ software and converted into micrometers using the scale bars created by the microscope; Kb values were obtained by multiplying micrometers by the constant stretching factor 2.59. To calculate the progression of a single replication forks (fork speed), the ratio between the green trait length (in Kb) and the time of IdU incubation (in minutes) was calculated. The inter-origin distance (IOD) (the length between two adjacent replication initiation sites) was determined by measuring centre-to-centre distances between two adjacent progressing forks (in Kb). The ratio between the lengths of the right and left nascent strands from the same origin was calculated to assess fork symmetry ($\geq$0.6) or asymmetry (<0.6).

QUANTIFICATION AND STATISTICAL ANALYSIS

Quantification

Densitometric analysis of Western Blotting experiments were performed using Image J software.

Statistics

Two-tailed unpaired Student's t test and one- two-way ANOVA for repeated measures were usedas detailed in the Figure legend. Number of cells used in clonogenic assay and in calcein test has been indicated in each specific methods section. Number of animals used in DSS treatment experiment has been indicated in Figure Legend. Differences were considered significant when p was less than 0.05. All statistical analyses were carried out using GraphPad Instat software (version 3.06.3).

Cell Reports, Volume *40*

Supplemental information

NCOA4 links iron bioavailability to DNA metabolism

Giorgia Federico, Federica Carrillo, Francesca Dapporto, Mario Chiariello, Massimo Santoro, Roberto Bellelli, and Francesca Carlomagno

Figure S1

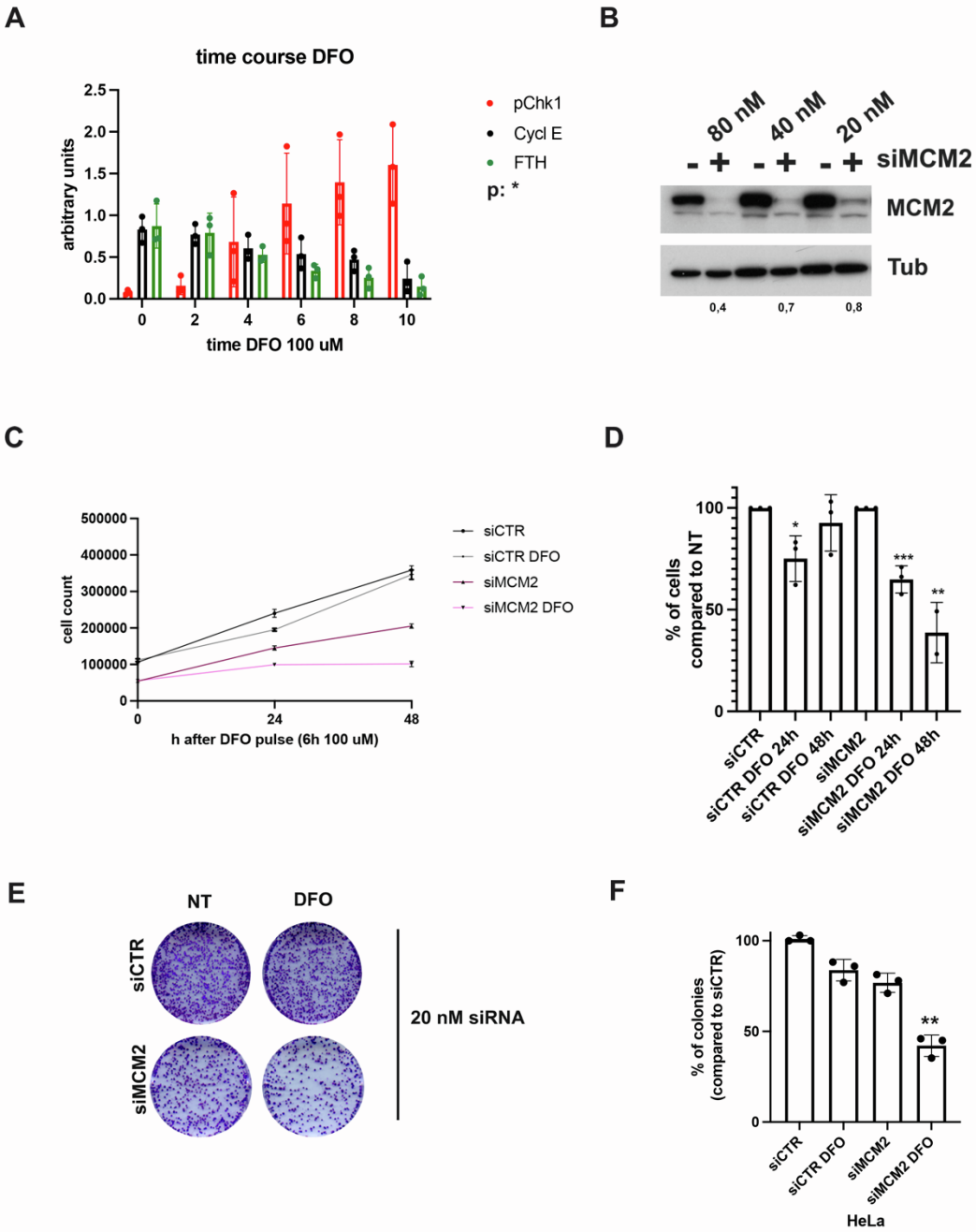
A
time course DFO
arbitrary units
2.5
2.0
1.5
1.0
0.5
0.0
0
2
4
6
8
10
time DFO 100 uM
pChk1
Cycl E
FTH
p: *
B
80 nM
40 nM
20 nM
- + - + - + siMCM2
MCM2
Tub
0,4
0,7
0,8
C
cell count
500000
400000
300000
200000
100000
0
0
24
48
h after DFO pulse (6h 100 uM)
siCTR
siCTR DFO
siMCM2
siMCM2 DFO
D
% of cells compared to NT
100
50
0
*
***
**
siCTR
siCTR DFO 24h
siCTR DFO 48h
siMCM2
siMCM2 DFO 24h
siMCM2 DFO 48h
E
NT
DFO
siCTR
siMCM2
20 nM siRNA
F
% of colonies (compared to siCTR)
100
50
0
**
siCTR
siCTR DFO
siMCM2
siMCM2 DFO
HeLa

Supplementary Figure S1. Iron depletion affects DNA replication and promotes replication stress, related to Figure 1.

(A) Scatter plot representing the densitometric analysis of western blot related to Figure 1B of the indicated proteins. Tubulin was used as loading control for Cyclin E and FTH whereas Chk1 was used as a loading control for pChk1. Each dot represents a single experiment. Three independent experiments were quantified. One-Way ANOVA was performed by comparing the mean of each group of treatment (NT vs DFO) at each time point. *=p <0,05. **(B)** Western blot analysis of MCM2 levels in HeLa cells after 48h of transfection with the indicated concentration of siRNA control (siCTR) and siRNA against MCM2 (siMCM2). **(C)** Growth curve of siCTR and siMCM2 HeLa cells. Cells were transfected with 20nM of siCTR or siMCM2. After 48h cells were treated for 6 hours with 100 uM Deferoxamine (DFO) or left in complete medium. Cells were count after 24 and 48h using an automatic cell counter (Biorad). **(D)** Scatter plot of the experiment described in Figure S1 C. Cell count was represented as the percentage of treated cells compared to untreated cells at each time point. Each dot represents a different experiment. Three independent experiments were plotted. T test analysis was done by comparing treated versus untreated cells. **(E)** Representative images of Clonogenic Assay of siCTR and siMCM2 HeLa cells. HeLa cells were transfected with 20nM of siCTR or siMCM2. After 48h 1000 cells were plated and treated or not with 1 mM DFO and then counted after 15 days. **(F)** Scatter plot of Clonogenic Assay described in Figure S1E. After 12 days colonies derived from siCTR and siMCM2 HeLa cells were counted and the percentage of treated-colonies compared to siCTR untreated colonies were represented. T test analysis was performed by comparing DFO-treated siMCM2 cells versus untreated siCTR cells. *= p<0,05; **= p<0,01; ***= p>0,001.

Figure S2

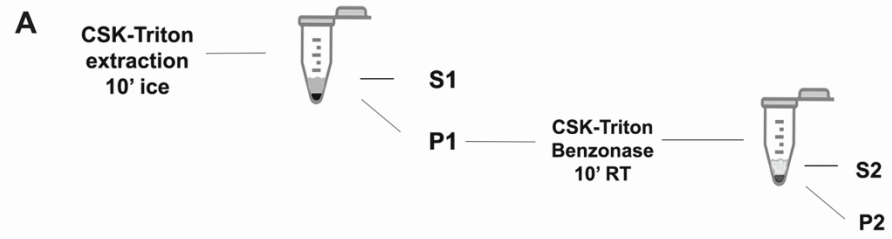
A
CSK-Triton
extraction
10' ice
S1
P1
CSK-Triton
Benzonase
10' RT
S2
P2

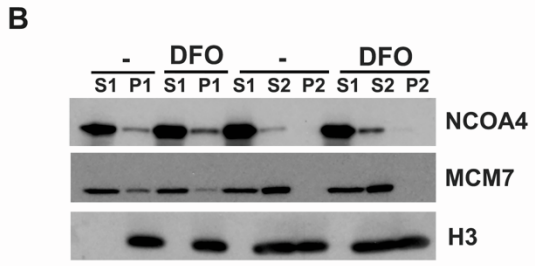
B
-
DFO
-
DFO
S1 P1 S1 P1 S1 S2 P2 S1 S2 P2
NCOA4
MCM7
H3

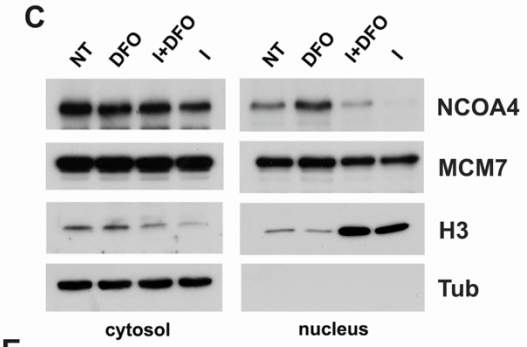
C
NT
DFO
I+DFO
I
NT
DFO
I+DFO
I
NCOA4
MCM7
H3
Tub
cytosol
nucleus

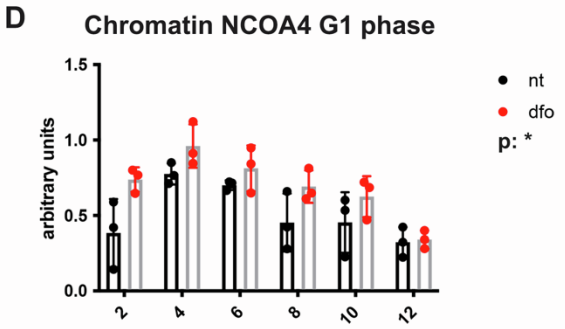
D
Chromatin NCOA4 G1 phase
arbitrary units
1.5
1.0
0.5
0.0
2
4
6
8
10
12
nt
dfo
p: *

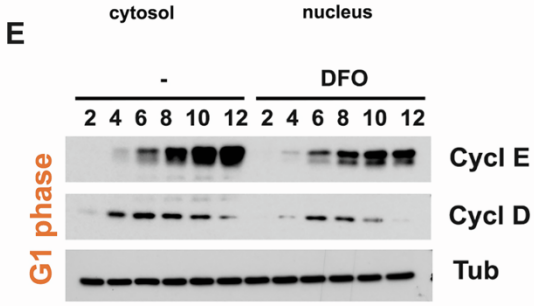
E
-
DFO
2 4 6 8 10 12 2 4 6 8 10 12
G1 phase
Cycl E
Cycl D
Tub

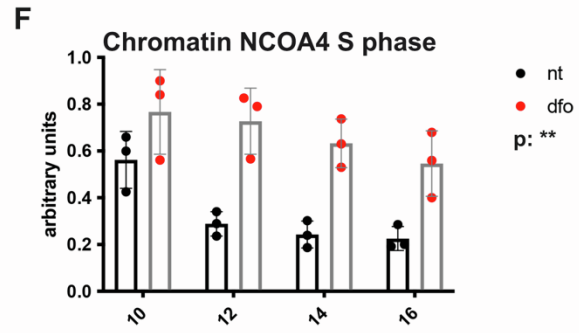
F
Chromatin NCOA4 S phase
arbitrary units
1.0
0.8
0.6
0.4
0.2
0.0
10
12
14
16
nt
dfo
p: **

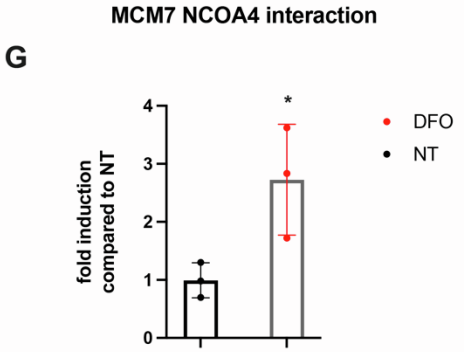
MCM7 NCOA4 interaction
G
fold induction
compared to NT
4
3
2
1
0
*
DFO
NT

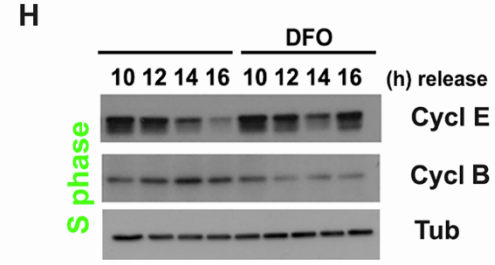
H
DFO
10 12 14 16 10 12 14 16 (h) release
S phase
Cycl E
Cycl B
Tub

Supplementary Figure S2. Intracellular iron levels control NCOA4 nuclear function, related to Figure 2.

(A) Schematic representation of the method used for cell fractionation and chromatin bound protein extraction. Cells were washed with PBS and extracted with CSK buffer (see Material and Methods) for 10 min on ice and then subjected to centrifugation (3000 rpm for 5 min). Two fractions were obtained: the supernatant fraction (S1) representing the CSK-soluble fraction and the pellet (P1) representing the CSK-insoluble fraction. In all the experiments shown the pellet P1 was dissolved in SDS loading buffer. When specified, the P1 fraction was further digested for 10 minutes in 100 ul CSK buffer containing Benzonase DNase to release chromatin-bound proteins from DNA. After 10 minutes centrifugation at 12300 rpm two fractions were obtained: S2 supernatant fraction representing the released proteins from DNA and the pellet P2 containing fragmented DNA and histones. **(B)** Western blot analysis of NCOA4, MCM7 and Histone H3 proteins extracted from HeLa cells treated or not for 2h with DFO (100 μM) following cell fractionation procedure as described in Figure S2A. S1 and P1: soluble and pellet (chromatin) fractions; S2 and P2: soluble and pellet fractions upon Benzonase digestion of P1. **(C)** Western blot analysis of NCOA4, MCM7, Histone H3 and tubulin in HeLa cells. Cells were treated for 2 h with DFO (100 μM) or vehicle in combination or not with a α/β importin inhibitor Ivermectin (25 nM). Cells were harvested and subjected to cytoplasmic and nuclear protein extraction by using Ne-PER kit (Thermofisher Scientific). Histone H3 and tubulin were used as a marker of cellular fractionation. **(D)** Scatter plot representing the densitometric analysis of western blot related to Figure 2C of NCOA4-chromatin bound protein of G1-phase HeLa cells. Cells were initially synchronized in M-phase by Nocodazole arrest and released in complete medium. Then after 2 h cells were treated with DFO (100 μM) and harvested at the indicated time point during G1-phase. Chromatin bound protein were extracted following cell fractionation described in Figure S2A. H3 was used as loading control. Each dot represents a different experiment. 3 independent experiments were quantified. Two-Way ANOVA was performed by comparing the mean of each group of treatment (NT vs DFO) at each time point. *=p <0,05. **(E)** Western blot analysis of cyclin E and D in the cytosolic fraction of G1-phase HeLa cells. Cells were initially synchronized in M-phase by Nocodazole arrest and released in complete medium. After 2 hours cells were treated with DFO (100 μM) and harvested at indicated time points. **(F)** Scatter plot representing the densitometric analysis of western blot related to Figure 2D of NCOA4-chromatin bound protein in S-phase HeLa cells. Cells were initially synchronized in M-phase by Nocodazole arrest and released in complete medium. After 8 hours cells were treated with DFO (100 μM) and harvested at indicated time points. Chromatin bound protein were extracted following cell fractionation described in Figure S2A. H3 was used as loading control. Each dot represents a different experiment. 3 independent experiments were quantified. Two-Way ANOVA was performed by comparing the mean of each group of treatment (NT vs DFO) at each time point. **=p <0,01. **(G)** Scatter plot representing the densitometric analysis of western blot related to Figure 2E of immunoprecipitated (IP NCOA4) NCOA4 and MCM7 proteins from HeLa cells

treated with vehicle or 100 μM DFO for 2 hours. Each dot represents a different experiment. 3 independent experiments were quantified and the ratio between DFO-treated and untreated cells was plotted. T Test *= p<0,05. **(H)** Western blot analysis of cyclin E and B in the cytosolic fraction of S-phase HeLa cells. Cells were initially synchronized in M-phase by Nocodazole arrest and released in complete medium. After 8 hours cells were treated with DFO and harvested at indicated time points.

Figure S3

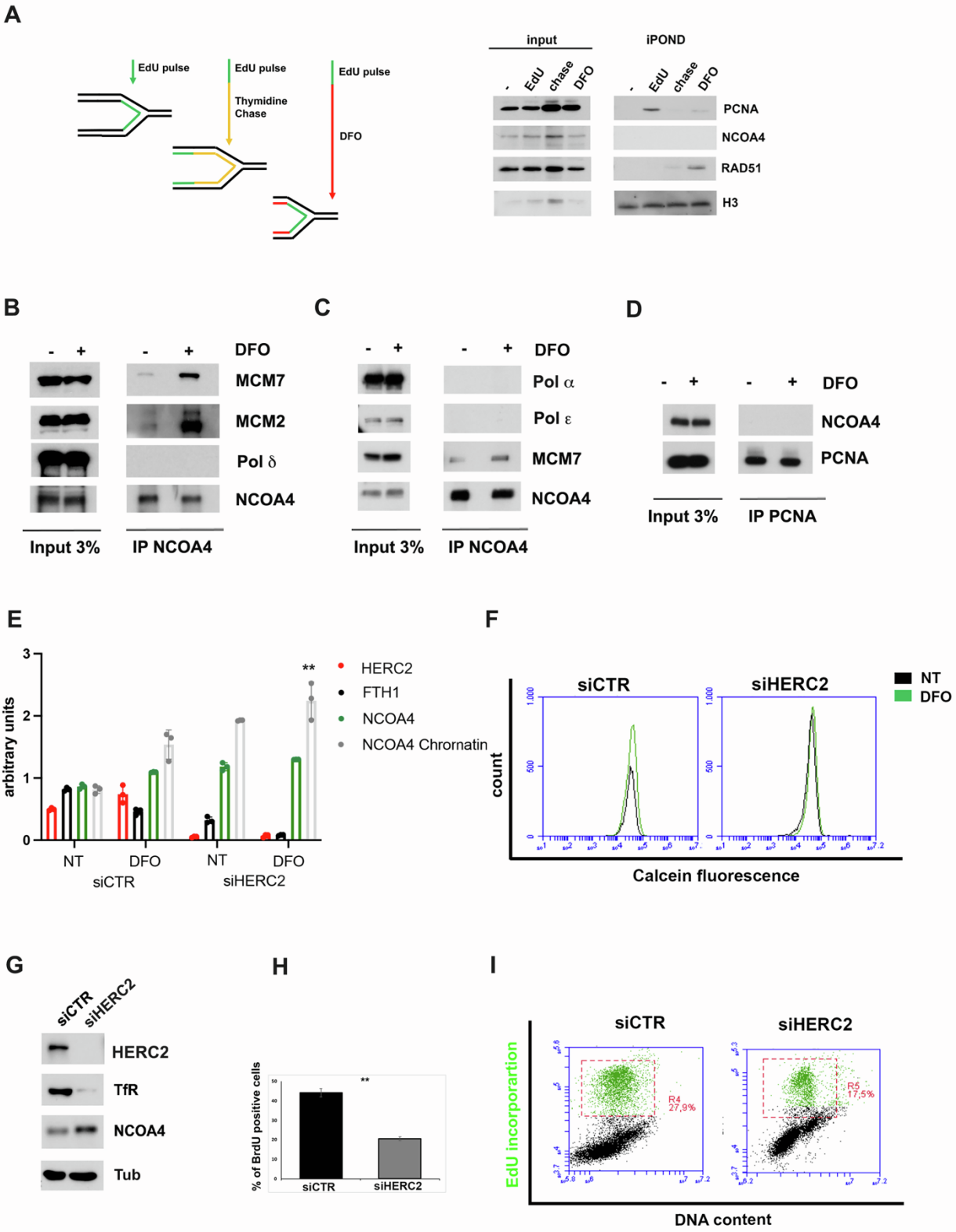
A
EdU pulse
EdU pulse
Thymidine Chase
EdU pulse
DFO
input
iPOND
-
EdU
chase
DFO
PCNA
NCOA4
RAD51
H3
B
DFO
MCM7
MCM2
Pol δ
NCOA4
Input 3%
IP NCOA4
C
Pol α
Pol ε
MCM7
NCOA4
D
NCOA4
PCNA
IP PCNA
E
arbitrary units
HERC2
FTH1
NCOA4
NCOA4 Chromatin
NT
DFO
siCTR
siHERC2
F
siCTR
siHERC2
NT
DFO
count
Calcein fluorescence
G
siCTR
siHERC2
HERC2
TfR
NCOA4
Tub
H
% of BrdU positive cells
I
siCTR
siHERC2
EdU incorporartion
R4
27,9%
R5
17,5%
DNA content

Supplementary Figure S3. Iron depletion promotes NCOA4 binding to unfired origins by preventing HERC2-dependent protein turn over, related to Figure 2.

(A) Left: Schematic representation of iPOND protocol used to evaluate NCOA4 presence at ongoing forks (EdU pulse), at a distant point from the moving replication fork (EdU pulse + thymidine chase) or at DFO-stalled forks (EdU pulse + DFO treatment). Right: Western blot analysis of indicated proteins isolated by iPOND assay. HeLa cells were pulse-labeled with EdU for 10 minutes (second lane) and then chased with thymidine for 30 minutes (third lane) or with DFO (100 μM) for 2 hours (fourth lane). In no-click samples (-), biotin azide was replaced by DMSO. **(B)** Western blot analysis of total (input 3%) and immunoprecipitated (IP NCOA4) MCM7, MCM2, DNApol δ and NCOA4 proteins from HeLa cells treated with vehicle (-) or 100 μM DFO (+) for 2 hours. **(C)** Western blot analysis of total (input 3%) and immunoprecipitated (IP NCOA4) MCM7, DNApol ε DNApol α and NCOA4 proteins from HeLa cells treated with vehicle (-) or 100 μM DFO (+) for 2 hours. **(D)** Western blot analysis of total (input 3%) and immunoprecipitated (IP NCOA4) PCNA and NCOA4 proteins from HeLa cells treated with vehicle (-) or 100 μM DFO (+) for 2 hours. **(E)** Scatter plot representing the densitometric analysis of western blot related to Figure 2F of the indicated proteins from soluble and chromatin fractions of HeLa cells transfected with control siRNA (siCTR) or siRNA against the HERC2 ubiquitin ligase (siHERC2) and treated with vehicle (-) or 100 Propidium Iodide DFO (+) for 2 hours. H3 and tubulin were used as loading control for soluble and insoluble fraction respectively. Each dot represents a different experiment. 3 independent experiments were quantified. T Test NCOA4-chromatin bound signal in siCTR (control) vs siHERC2 (against HERC2 protein) cells **=p <0,01. **(F)** Representative histogram plot of Calcein fluorescence in HeLa cells transfected with siRNA control or siRNA against HERC2 protein. After 48h of transfection, cells were treated with DFO (1 mM) and Calcein fluorescence was analyzed at cytofluorimeter. Calcein fluorescence is normally quenched by free iron. The differences between DFO-treated and untreated cell fluorescence were calculated and indicated as Labile Iron Pool. **(G)** Western blot analysis of the indicated proteins extracted from HeLa cells transfected with siCTR (control) control or siHERC2 (against HERC2 protein)**. (H)** Quantification of BrdU staining in HeLa cells transfected for 48h with siCTR or siHERC2. Cells were incubated for 30 minutes with BrdU and then analyzed by immunofluorescence using 5-Bromo-2′-deoxy-uridine Labeling and Detection Kit. T Test p= ** <0,01. (**I**) Representative dot plot of EdU incorporation (green fluorescence) vs Propidium Iodide staining (red fluorescence) analyzed by FACS in HeLa cells transfected for 48h with siCTR or siHERC2.

Figure S4

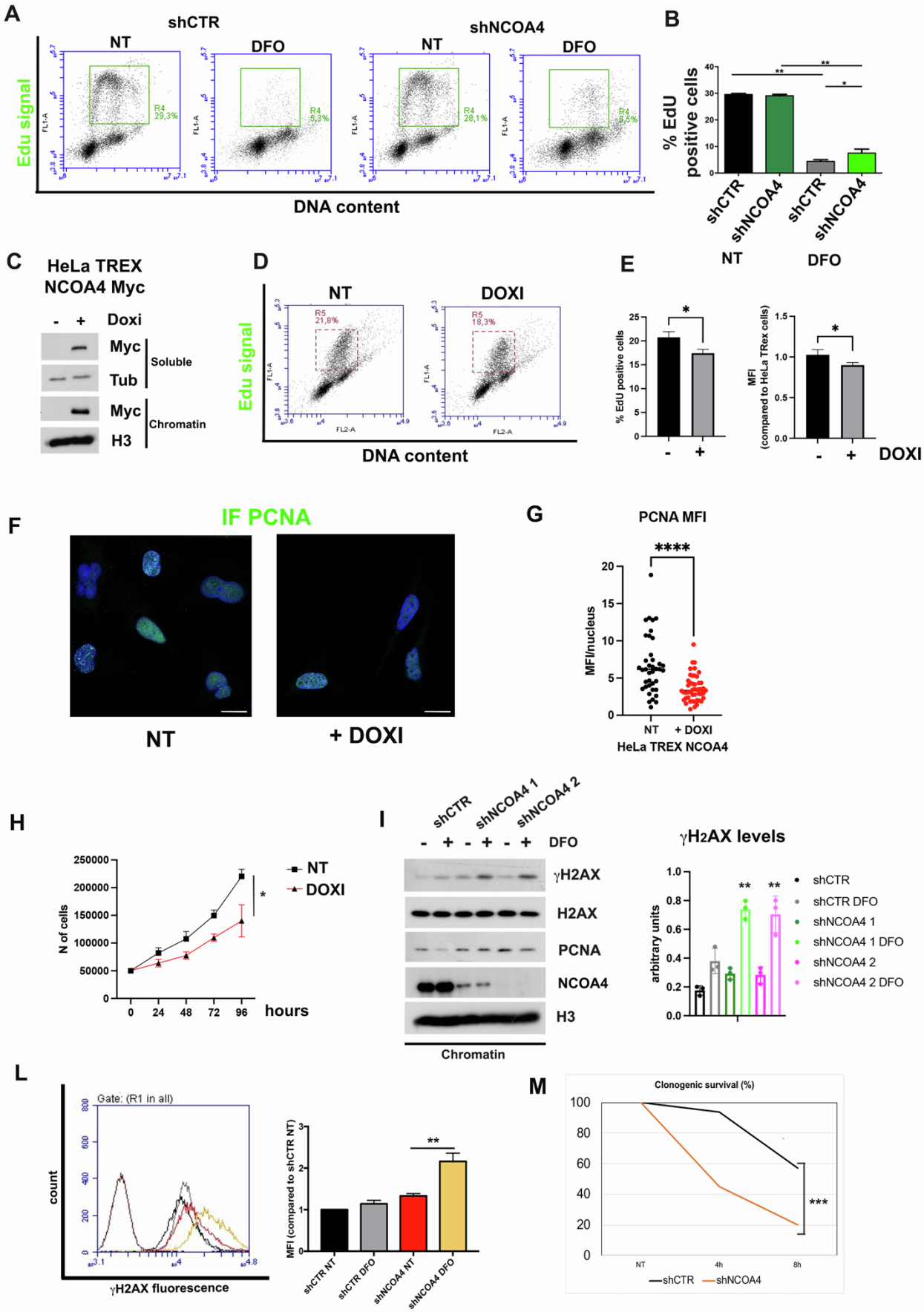
A
shCTR
shNCOA4
NT
DFO
NT
DFO
Edu signal
DNA content
R4 29,3%
R4 5,3%
R4 28,1%
R4 5,5%
B
% EdU positive cells
shCTR
shNCOA4
shCTR
shNCOA4
NT
DFO
C
HeLa TREX NCOA4 Myc
- + Doxi
Myc
Tub
Soluble
Myc
H3
Chromatin
D
NT
DOXI
Edu signal
DNA content
R5 21,8%
R5 18,3%
E
% EdU positive cells
MFI (compared to HeLa TRex cells)
- +
DOXI
F
IF PCNA
NT
+ DOXI
G
PCNA MFI
MFI/nucleus
NT
+ DOXI
HeLa TREX NCOA4
H
N of cells
hours
NT
DOXI
I
shCTR
shNCOA4 1
shNCOA4 2
DFO
γH2AX
H2AX
PCNA
NCOA4
H3
Chromatin
γH2AX levels
arbitrary units
shCTR
shCTR DFO
shNCOA4 1
shNCOA4 1 DFO
shNCOA4 2
shNCOA4 2 DFO
L
Gate: (R1 in all)
count
γH2AX fluorescence
MFI (compared to shCTR NT)
shCTR NT
shCTR DFO
shNCOA4 NT
shNCOA4 DFO
M
Clonogenic survival (%)
NT
4h
8h
shCTR
shNCOA4

Supplementary Figure S4. NCOA4 restrains activation of new origins in iron depletion and prevents replication stress in low iron conditions, related to Figure 3.

(A) Flow cytometry analysis of EdU incorporation vs Propidium Iodide staining (DNA content) of shCTR and shNCOA4 HeLa cells in normal (NT) and iron depleted (DFO100 μM) conditions (6h). **(B)** Bar graph showing the percentage of the EdU positive shCTR and shNCOA4 cells treated as described in S4A. Mean values ± standard deviation of 3 experiments were represented. *p<0,05; ** p<0,01. **(C)** Western blot analysis of the indicated proteins in soluble and chromatin fraction extracted from HeLa cells stably expressing the tetracycline repressor protein (T-REx™ HeLa cells) and the inducible vector pcDNA™4 NCOA4 Myc. Cells were treated with Doxycycline for 48 h to allow NCOA4 Myc expression and then lysed following cell fractionation as described in S2A. **(D)** Flow cytometry analysis of EdU incorporation vs Propidium Iodide staining (DNA content) of HeLa cells stably expressing the tetracycline repressor protein and the inducible vector pcDNA™4 NCOA4 Myc (HeLa T-REx™ NCOA4 Myc) treated (DOXI) or not (NT) with Doxycycline for 48 h. **(E)** Left: Bar graph showing the percentage of the EdU positive HeLa T-REx™ NCOA4 Myc cells treated (DOXI) or not (NT) with Doxicycline for 48 h as described in S4D. Right: Bar graph showing the ratio between Mean Fluorescence Intensity (MFI) of HeLa T-REx™ NCOA4 Myc cells Doxicycline-treated (+) versus HeLa T-REx™ NCOA4 Myc untreated (-) cells. MFI values ± standard deviation of 3 experiments were represented. *p<0,05. **(F)** Representative images of confocal immunofluorescent analysis of PCNA foci in HeLa T-REx™ NCOA4 Myc cells treated (+ DOXI) or not (NT) with Doxicycline for 48h. Scale bar 10 μm. **(G)** Bar graphs showing PCNA intensity staining vs nuclei area of HeLa T-REx™ NCOA4 Myc cells treated or not with Doxicycline for 48 h as in S4F. **(H)** Growth curve of HeLa T-REx™ NCOA4 Myc cells grown in presence (DOXI) or not (NT) of Doxicycline. 5 x 10^4 cells were plated and counted every 24h by using automatic cell counter (Biorad). Two-Way ANOVA was performed by comparing the mean of each group of cells (not treated vs Doxicycline treated) at each time point. ****=p <0,0001. **(I)** Left: Western blot analysis of the indicated proteins in chromatin fraction extracted from HeLa shCTR cells and two different shNCOA4 clone cells (shNCOA4 1 and shNCOA42 cells). Cells were initially synchronized in M-phase by Nocodazole arrest and released in complete medium. Then after 8 hours cells were treated for 2 hours with DFO (100 μM) and then harvested. Right: Scatter plot representing the densitometric analysis of western blot related to S4I (left) of the indicated proteins. H3 was used as loading control. Each point represents a different experiment. 3 independent experiments were quantified. T Test **=p <0,01. **(L)** Left: representative histogram plot of γH2AX fluorescence in shCTR and shNCOA4 cells. Asynchronous cells were treated for two hours with DFO (100 uM) and γH2AX signal was evaluated by flow cytometry using anti-γH2AX fluorescein antibody. Right: quantification of the Mean Fluorescence Intensity of γH2AX signal derived from 3 independent experiment.

Data are represented as fold increase compared to shCTR NT cells. **(M)** Clonogenic assay quantification. HeLa cells stably expressing shCTR and shNCOA4 were treated with 1 mM DFO (1 h) and then left for 12 days in culture. Colonies were counted after crystal violet staining and the percentage of colonies after treatment compared to untreated cells were calculated. p= * <0,05; ** <0,01; *** <0,001.

Figure S5

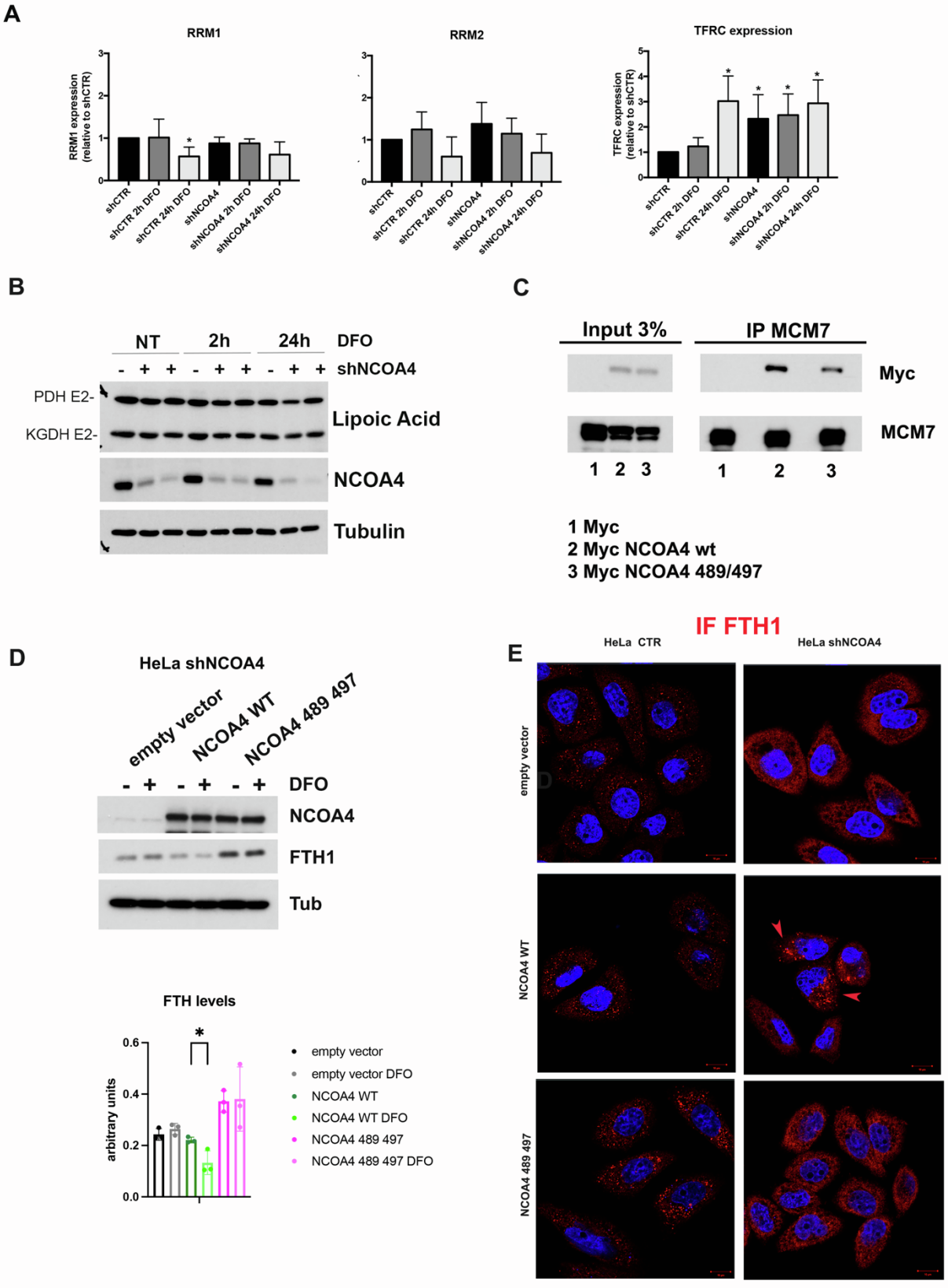
A
RRM1
RRM1 expression (relative to shCTR)
shCTR
shCTR 2h DFO
shCTR 24h DFO
shNCOA4
shNCOA4 2h DFO
shNCOA4 24h DFO
RRM2
TFRC expression
TFRC expression (relative to shCTR)
B
NT
2h
24h
DFO
shNCOA4
PDH E2-
KGDH E2-
Lipoic Acid
NCOA4
Tubulin
C
Input 3%
IP MCM7
Myc
MCM7
1 2 3
1 2 3
1 Myc
2 Myc NCOA4 wt
3 Myc NCOA4 489/497
D
HeLa shNCOA4
empty vector
NCOA4 WT
NCOA4 489 497
DFO
NCOA4
FTH1
Tub
FTH levels
arbitrary units
empty vector
empty vector DFO
NCOA4 WT
NCOA4 WT DFO
NCOA4 489 497
NCOA4 489 497 DFO
E
IF FTH1
HeLa CTR
HeLa shNCOA4
empty vector
NCOA4 WT
NCOA4 489 497

Supplementary Figure S5. NCOA4 deficiency does not affect iron-dependent enzymes, related to Figure 4.

(A) Bar graph representing the mRNA levels of the catalytic subunit of ribonucleotide reductase (RRM1), of the regulatory subunit of ribonucleotide reductase (RRM2) and of Transferrin receptor 1 (TFRC) in Hela shCTR and shNCOA4 stable clones not treated or after 2 and 24h of DFO treatment (100 uM). p= *< 0,05. **(B)** Western blot analysis of lipoic acid conjugated to PDH E2 (Pyruvate Dehydrogenase E2) and KGDH E2 (Alpha-ketoglutarate dehydrogenase), of shCTR and 2 different shNCOA4 stable clones not treated (-) or treated with DFO (100 uM) for 2 and 24h. Tubulin was used as loading control. **(C)** Total (input) and co-immunoprecipitated (IP MCM7) Myc-tagged NCOA4 and endogenous MCM7 proteins in HeLa shNCOA4 cells transiently transfected with Myc-empty vector, or vectors expressing sh-resistant Myc-NCOA4 or sh-resistant MYC NCOA4 489-497 mutant. **(D)** Upper: western blot analysis of FTH1 and NCOA4 protein levels in HeLa shNCOA4 cells transiently transfected with Myc-empty vector, or vectors expressing sh-resistant Myc-NCOA4 or sh-resistant MYC NCOA4 489-497 mutant treated or not with DFO (100 μM). Lower part: Scatter plot representing the densitometric analysis of western blot related to D of the indicated proteins. Each dot represents a different experiment. 3 independent experiments were quantified. p= *< 0,05. **(E)** Representative images of confocal immunofluorescent analysis of FTH1 in shCTR and shNCOA4 HeLa cells transfected with Myc-empty vector, or vectors expressing sh-resistant Myc-NCOA4 or sh-resistant MYC NCOA4 489-497 mutant. Cells were treated with Ferric Ammonium Acetate (FAC) for 12h and to promote ferritinophagy, cells were then washed and treated with DFO (100 μM) plus Cloroquine (autophagy inhibitor) for 6 hr. Cells were fixed, stained with FTH1 antibody and visualized by confocal microscopy. Scale bar, 10 μm. Arrows indicate ferritin accumulation in lysosomes.

Figure S6

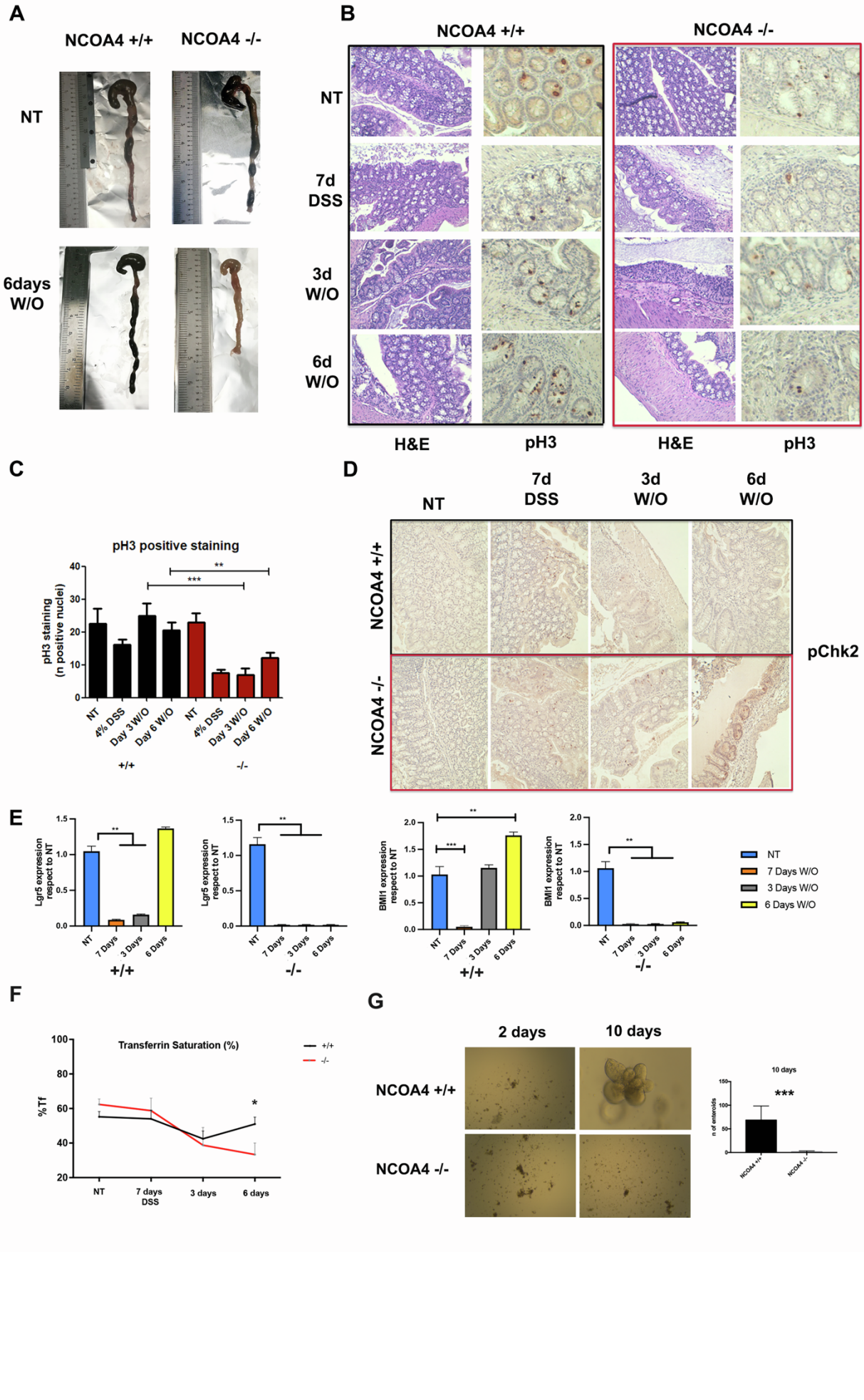
A
NCOA4 +/+
NCOA4 -/-
NT
6days W/O
B
NCOA4 +/+
NCOA4 -/-
NT
7d DSS
3d W/O
6d W/O
H&E
pH3
H&E
pH3
C
pH3 positive staining
pH3 staining (n positive nuclei)
NT
4% DSS
Day 3 W/O
Day 6 W/O
+/+
-/-
D
NT
7d DSS
3d W/O
6d W/O
NCOA4 +/+
NCOA4 -/-
pChk2
E
Lgr5 expression respect to NT
BMI1 expression respect to NT
NT
7 Days
3 Days
6 Days
+/+
-/-
NT
7 Days W/O
3 Days W/O
6 Days W/O
F
Transferrin Saturation (%)
%Tf
+/+
-/-
NT
7 days DSS
3 days
6 days
G
2 days
10 days
NCOA4 +/+
NCOA4 -/-
10 days
n of enteroids

Supplementary Figure S6. NCOA4 null mice are hypersensitive to DSS treatment and show impaired intestinal regeneration, related to Figure 5.

(A) Representative macroscopic image of colons derived from NCOA4 +/+ and -/- mice untreated (NT) or sacrificed after 6 days of wash out (6 W/O) from treatment with DSS (4% for 7 days). **(B)** Representative images of hematoxylin and eosin (H&E) and immunohistochemistry staining for phospho-H3 protein (p-H3) of colon sections derived from NCOA4 +/+ and -/- mice. Mice were sacrificed after 7 days of DSS treatment (7d DSS) and after 3 or 6 days of wash/out (3 W/O, 6 W/O). Untreated mice were used as control (NT). **(C)** Histogram representing the number of intestinal cells showing nuclear signal for phospho-H3 protein (p-H3) in NCOA4 +/+ and -/- mice treated as in S6B. p-H3 positive cells were counted in 20X power field. 10 fields per mice were analysed for each time point as described in B. **(D)** Representative images of phospho-Chk2 immunoistochemistry derived from colon sections of NCOA4 +/+ and -/- mice. Mice were sacrificed after 7 days of DSS treatment (7d DSS) and after 3 (3d W/O) or 6 (6d W/O) days of wash/out. Untreated mice were used as control (NT). **(E)** mRNA expression measured by rt-PCR of LGR5 and BMI gene in NCOA4 +/+ and -/- mice treated as in S6B. **(F)** Transferrin saturation of NCOA4 -/- and +/+ mice treated as described in S6B **(G)**. NCOA4 -/- and +/+ mice were treated with DSS 4% for 7 days then DSS was replaced by normal water to allow intestinal regeneration. Mice were sacrificed after 6 days of wash/out and colonic crypts from large intestine were isolated and cultured for 10 days in Matrigel. representative images of intestinal organoids derived from NCOA4 -/- and +/+ mice after 2 and 10 days in 3D culture. low panel right: histograms representing the mean number of intestinal organoids per well after 10 days of growth in Matrigel. p= ** <0,01; p=*** <0,001